NOAA Technical Memorandum OAR GSD-61
https://doi.org/10.25923/n9wm-be49

A Description of the MYNN-EDMF Scheme and the Coupling to Other Components in WRF–ARW

March 2019

Joseph B. Olson
Jaymes S. Kenyon
Wayne. A. Angevine
John M. Brown
Mariusz Pagowski
Kay Sušelj

Earth System Research Laboratory
Global Systems Division
Boulder, Colorado
March 2019

noaa NATIONAL OCEANIC AND ATMOSPHERIC ADMINISTRATION / Office of Oceanic and Atmospheric Research

NOAA Technical Memorandum OAR GSD-61

A Description of the MYNN-EDMF Scheme and the Coupling to Other Components in WRF–ARW

Joseph B. Olson[1,2],
Jaymes S. Kenyon[1,2],
Wayne. A. Angevine[1,4],
John M. Brown[2],
Mariusz Pagowski[1,2],
Kay Sušelj[3]

[1] Cooperative Institute for Research in Environmental Sciences (CIRES) and NOAA/ESRL/GSD

[2] National Oceanic and Atmospheric Administration, Earth System Research Laboratory, Global Systems Division (NOAA/ESRL/GSD)

[3] Jet Propulsion Laboratory, National Aeronautics and Space Administration (NASA), Pasadena, California

[4]National Oceanic and Atmospheric Administration, Earth System Research Laboratory, Chemical Sciences Division (NOAA/ESRL/CSD)

Acknowledgements

The authors would like to thank Dr. Mikio Nakanishi for sharing the original version of the MYNN PBL scheme and offering helpful insight and advice as the scheme was developed in WRF-ARW. Funding for this work was provided by many sources, each helping to develop different components of the MYNN-EDMF scheme. These agencies/programs include NOAA's Atmospheric Science for Renewable Energy (ASRE) program, the Federal Aviation Administration (FAA), NOAA's Next Generation Global Prediction System (NGGPS), and the U.S. DOE Office of Energy Efficiency and Renewable Energy Wind Energy Technologies Office. The views expressed are those of the authors and do not necessarily represent the official policy or position of any funding agency. We are grateful to the National Center for Atmospheric Research Mesoscale and Microscale Meteorology Laboratory (http://www.mmm.ucar.edu/wrf/users), which is responsible for the Weather Research and Forecasting Model, and specifically grateful for help from Jimy Dudhia, Wei Wang, and Dave Gill.

UNITED STATES DEPARTMENT OF COMMERCE

Wilbur Ross
Secretary

NATIONAL OCEANIC AND ATMOSPHERIC ADMINISTRATION

Benjamin Friedman
Acting Under Secretary for Oceans
And Atmosphere/NOAA Administrator

Office of Oceanic and Atmospheric Research

Craig N. McLean
Assistant Administrator

Contents

1. Introduction

The Mellor–Yamada–Nakanishi–Niino (MYNN) (Nakanishi and Niino 2001, 2004, 2006, and 2009) scheme was first integrated into the Advanced Research version of the Weather Research and Forecasting Model (WRF-ARW) version 3.1 (Skamarock et al. 2008) by Mariusz Pagowski of the National Oceanic and Atmospheric Administration (NOAA) Global Systems Division (GSD). The purpose of this addition was to introduce an alternative turbulent kinetic energy (TKE)-based planetary boundary layer (PBL) scheme which could serve as a candidate PBL parameterization for NOAA's operational Rapid Refresh (RAP; Benjamin et al. 2016) and High-Resolution Rapid Refresh (HRRR) forecast systems. Both systems employ WRF–ARW as the model component of the forecast system.

The MYNN scheme was demonstrated to be an improvement over predecessor Mellor–Yamada-type PBL schemes (e.g., Mellor and Yamada 1974, 1982) when compared against large-eddy simulations (LES) of a convective PBL (Nakanishi and Niino 2004, 2009), the prediction of advection fog (Nakanishi and Niino 2006), and for the representation of coastal barrier jets (Olson and Brown 2009). The MYNN scheme, designed to function at either level 2.5 or 3.0 closure, includes a partial-condensation scheme (also known as a *cloud PDF* or a *statistical-cloud scheme*) to represent the effects of subgrid-scale (SGS) clouds on the buoyancy flux (Nakanishi and Niino 2004, 2006, and 2009). The closure constants for the original MYNN scheme were tuned to a database of LES as opposed to observational data. Numerous turbulence statistics can be obtained throughout the entire PBL under controlled conditions using LES; a potential advantage. The idealized conditions exclude irregularities caused by nonstationary, transitional, or mesoscale phenomena, as well as measurement inaccuracies, which may contaminate observed data (e.g., Esau and Byrkjedal 2007).

Since implementation into WRF–ARW, the MYNN scheme has been extensively modified, largely driven by requirements to improve forecast skill in support of the NOAA's National Weather Service (NWS), the Federal Aviation Administration (FAA) and users within the renewable-energy industry. Specifically, fundamental changes were made to the formulation of the mixing lengths and representation of SGS clouds, but new components have also been added to improve the representation of nonlocal mixing, the interaction with clouds, and the coupling to other model components in WRF−ARW. This manuscript serves as a description of the MYNN scheme as it has evolved within WRF−ARW since the original implementation. Hereafter, the original MYNN scheme, as described by Nakanishi and Niino (2009), will be referred to as MYNN, and the present-day MYNN scheme (as of this date of this memorandum), which uses an eddy-diffusivity / mass-flux (EDMF) approach, will be referred to as the MYNN-EDMF.

2. Formulation of the Eddy-Diffusivity Component

The local component of the turbulent fluxes of θ_{li}, q_x, and momentum throughout the entire atmosphere are computed using an eddy-diffusivity approach. This approach uses an eddy-diffusivity coefficient K_h for the thermal and moisture variables and an eddy-viscosity coefficient K_m for the horizontal velocity components. The turbulent fluxes are represented as a product of the local gradient of ϕ (between adjacent model layers) and an eddy-diffusivity coefficient:

$$\overline{w'\phi'} = -K_{h,m}\left(\frac{\partial \phi}{\partial z} - \gamma\right), \quad (1)$$

where ϕ can be any scalar or momentum component and the counter-gradient term, γ, is a function of the higher order moments, so it is only used in the level-3 closure. The MYNN follows Mellor and Yamada (1982) in that the eddy-diffusivity and eddy-viscosity, K_h and K_m, respectively, are related to q [$q = (2{\cdot}TKE)^{1/2} = QKE^{1/2}$, where QKE is an important quantity in the MYNN code], a mixing-length scale (l), and stability functions S_h and S_m, as follows:

$$K_{h,m} = lqS_{h,m}. \quad (2)$$

The stability functions have different forms for each closure level, taking into account more higher-order terms as they become prognostic at higher-order closures (Mellor and Yamada 1982; Nakanishi and Niino 2004). A brief background to each of the individual components of K_h and K_m as well as modifications to these original components of the MYNN are described below.

2.1 The TKE Equation

Of foremost importance to any TKE-based eddy-diffusivity PBL scheme is the TKE equation, since TKE is a measure of turbulence intensity and is therefore directly related to the turbulent transport of momentum, heat, and water vapor in the atmosphere (e.g., Stull 1988). As such, TKE is often used in place of vertical-velocity variance in TKE-based PBL schemes. In the MYNN, the TKE equation takes the form of:

$$\frac{\partial q^2}{\partial t} = \frac{\partial}{\partial z}\left[lqS_q\frac{\partial q}{\partial z}\right] + P_s + P_b + D, \quad (3)$$

where the advection of TKE by the resolved-scale flow is neglected in (3), but available as a feature in WRF-ARW (described at the end of this section). The first term on the right-hand side of (3) is the vertical transport term, and P_s, P_b, and D refer respectively to shear production, buoyancy production/destruction, and dissipation. Only slight behavioral changes to the original MYNN are made to the vertical-transport term due to changes in the mixing length (described in the following subsection). The stability function for TKE, $S_q = 3S_m$, remains unchanged. This is usually larger than the constant $S_q = 0.2$ used in Mellor and Yamada (1982) and Janjić (2002) but smaller than $S_q = 5S_m$ used in Grenier and Bretherton (2001) and Bretherton et al. (2004). The second and fourth terms, relating to the shear production (P_s) and the dissipation (D) of TKE, respectively, also remain unchanged. Only the third term on the right-hand side, the buoyancy production/dissipation term P_b, has been modified to include the production of turbulence from cloud-top cooling.

In stratocumulus clouds, strong cloud-top cooling can make the upper cloud layer negatively buoyant, driving convective turbulence, even when the underlying surface fluxes are small (e.g., Deardorff 1980; Duynkerke and Driedonks 1987). In an attempt to incorporate this process into the TKE equation, the buoyancy production/destruction term,

$$P_b = 2\frac{g}{\theta_0}\left(\overline{w'\theta_v'}\right) \quad (4)$$

is modified, such that the heat flux, which was originally only a buoyancy flux (explained further in section 4), includes a new nonlocal production component (last term on the right):

$$\overline{(w'\theta_v')} = -\beta_\theta\overline{(w'\theta_l')} - \beta_q\overline{(w'q_w')} - A\left(\frac{\theta_v}{g}\right)\frac{w_l^3}{h}(h-z)\left(1-\frac{h-z}{h}\right)^3 \quad (5)$$

Where $A = 0.2(1 + a_2E)$ is the entrainment efficiency, taken from Nicholls and Turton (1986) except the value of a_2 is set to 8, following Wilson and Fovell (2018) and E is a function of vertical gradients of θ_l and q_c. The convective velocity scale w_l is defined as,

$$w_l = \left[\frac{g}{\theta}\left(\overline{w'\theta'}\right)_{z_i} z_i\right]^{1/3}, \quad (6)$$

but instead of using the heat flux at the surface, the heat flux associated with the radiative flux at the top of the cloud is used instead. The subscript and variable z_i correspond to the PBL height. The nonlocal nature of this new buoyancy production term is controlled by the linear-cubic vertical scaling function.

This new feature was added to the MYNN-EDMF in NOAA-GSD's WRF3.9 codebase as a potential candidate for future versions of the operational RAP/HRRR. It has also been added to NCAR's WRF–ARW repository for version 4.0, but is not activated by default, since this feature is still considered under development. To activate this feature, an integer parameter inside phys/module_bl_mynn.F, *bl_mynn_topdown* must be changed to 1.

Lastly, a unique feature of the MYNN-EDMF in WRF–ARW is the ability to advect the TKE. This feature is possible because TKE is defined on mass points (middle of layer — not at the interface) unlike most other TKE-based schemes in WRF–ARW. This allows the advection schemes in WRF–ARW to advect TKE like all other scalars defined on mass points. In early versions of the MYNN, the advection of TKE was known to cause numerical instabilities near lateral boundaries, especially when run at level 3, so TKE advection has not been activated for use in the operational RAP or HRRR. More recent versions have shown numerical stability, allowing this feature to be a candidate for inclusion in future versions of the RAP and HRRR. To activate this option, set the namelist parameter *bl_mynn_tkeadvect* to true (refer to Appendix).

A relatively new feature to the MYNN-EDMF is the contribution of heating due to the dissipation of TKE, which is parameterized as:

$$c_p \frac{\partial T}{\partial t} = d_1 D\ , \quad (7)$$

where T is the temperature, c_p is the specific heat of dry air at constant pressure, and D is the dissipation of TKE, using the same form as used in (3). The coefficient d_1 is set to 0.5. This is the same form used in the TKE-based EDMF scheme currently under development within the Global Forecast System (GFS) (Han and Bretherton 2019). The heating rate from (7) is multiplied by the time step, Δt, and added to the temperature profile prior to computing the tendencies by use of the implicit solver.

2.2 Mixing Lengths

The mixing lengths have been revised twice since the original implementation of the MYNN into WRF–ARW. Below is a brief summary of the original form and each successive revision. A new namelist parameter *bl_mynn_mixlength* has been added to WRF–ARW to easily switch between different mixing length formulations (refer to Appendix 1). A description of each formulation follows:

i. Original form: *bl_mynn_mixlength* = 0

The mixing length, l, is designed such that the shortest length scale among the surface-layer length, l_s, turbulent length, l_t, and buoyancy length, l_b, will dominate. The physical justification is that each length scale is associated with a turbulence-limiting factor, such as static stability, distance

from the surface, or integrated turbulence within the PBL. After all of the relevant mixing length scales are determined, they must be carefully blended to into a single mixing-length profile, which characterizes the mean displacement of a parcel by turbulent eddy mixing at any particular level. To obtain a blended mixing length at each model level, the original MYNN used a harmonic average,

$$\frac{1}{l} = \frac{1}{l_s} + \frac{1}{l_t} + \frac{1}{l_b} \tag{8}$$

As a consequence of the harmonic average, the resultant mixing length is always biased to be smaller than the smallest individual length scale. Alternative blending techniques have been tested in subsequent versions of the MYNN and will be discussed later in this section, but first, we overview the formulation and physical meaning of each individual length scale.

The surface-layer length scale l_s is meant to help regulate the turbulent mixing near the surface, where it is typically the smallest turbulence-limiting factor. In the MYNN, l_s is represented as a function of the surface stability parameter ($\zeta = z/L$), where L is the Obukhov length [$= -u_*^3\ \theta_{v0} / kg(w'\theta')$] and z is the height AGL:

$$l_s = \begin{cases} kz(1 + cns\zeta)^{-1}, & 0 \le \zeta \le 1 \\ kz(1 - \alpha_4\zeta)^{0.2}, & \zeta < 0 \end{cases} \tag{9}$$

where k is the von Karman constant (= 0.4), and the variables *cns* and α_4 allow the mixing length to vary with surface stability. Values of α_4 ranging from 10 to 100 allow l_s to become ~O(z) in unstable conditions and value of *cns* ranging from 2.1 to 3.5 reduces l_s to become significantly smaller than kz in very stable conditions. This makes the MYNN somewhat unique, departing from the most commonly used form, $l_s = kz$, which originates from Prandtl's mixing length hypothesis for neutral conditions. Despite this limited region of the validity for using kz, this approximation is nonetheless used across the entire spectrum of stability in many other PBL schemes. The general form of l_s has remained the same in the MYNN-EDMF, but the constants *cns* and α_4 have been modified (Fig. 1).

The general form of the turbulent length scale l_t is taken from Mellor and Yamada (1974) but is modified to become larger in magnitude:

$$l_t = \alpha_1 \frac{\int_0^\infty qz\ dz}{\int_0^\infty q\ dz}, \tag{10}$$

where q is defined above and $\alpha_1 = 0.23$ as opposed to 0.10 in Mellor and Yamada (1974). This mixing length scale typically dominates in the middle and upper portion of a convective boundary layer and can vary from 10–50 m in stable conditions to 100–500 m in unstable conditions; therefore, l_t can be thought of as an approximation for the size of the mean turbulent eddy in the

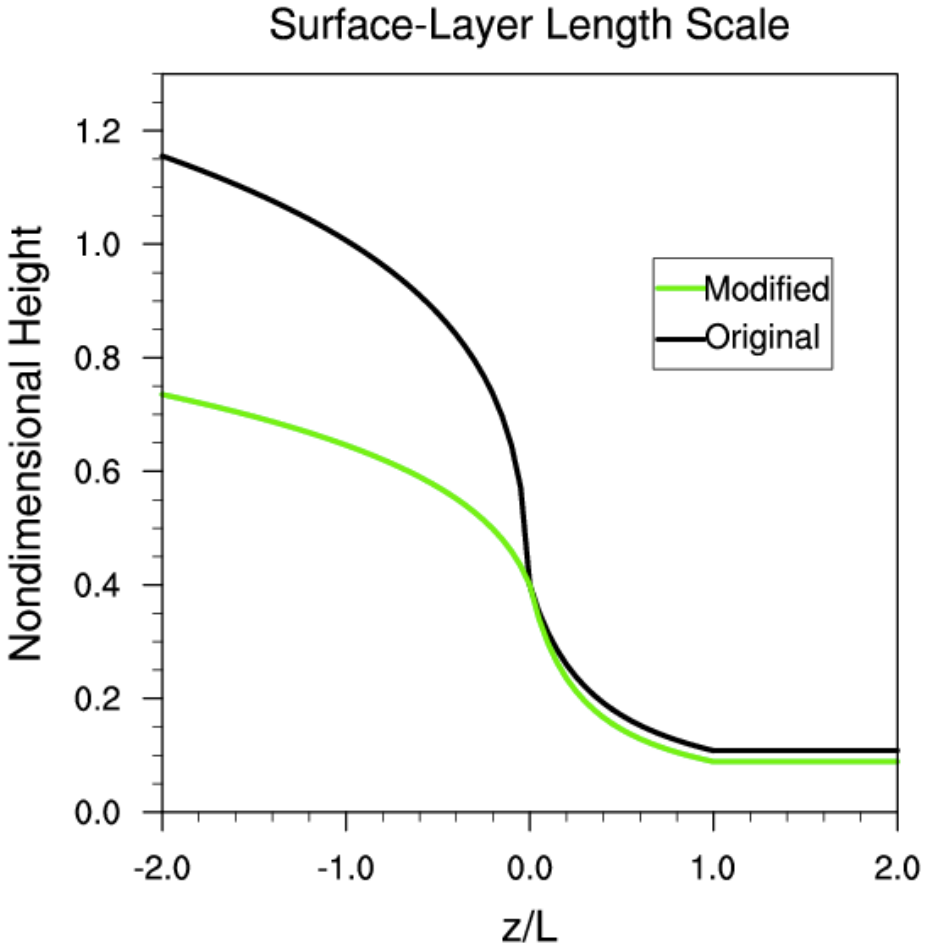

Figure 1. Modified (green) and original (black) surface-layer length scales. The green line shows equation 9 with updated values of cns = 3.5 and α_4 =10, while the black line has original values of cns = 2.7 and α_4 =100. A non-dimensional height of 0.4 is equivalent to $l_s = kz$, strictly valid only at neutral conditions ($z/L = 0$).

PBL. Note that in the original MYNN, this form was integrated from the surface to the top of the model atmosphere, taking into account TKE that is well above the PBL. This caused l_t to be occasionally diagnosed in excess of 2000 m, resulting in spurious large mixing. This was revised (discussed later in this section).

The buoyancy length scale l_b is:

$$l_b = \alpha_2 \frac{q}{N}\left[1 + \alpha_3 \left(\frac{q_c}{l_t N}\right)^{1/2}\right] \qquad (11)$$

where the Brunt-Väisälä frequency, $N = [(g/\theta_0)\partial\theta_v/\partial z]^{1/2}$ and $q_c = [(g/\theta_0)\langle w'\theta'_v\rangle\, g\, l_t]^{1/3}$, is a turbulent velocity scale, similar to the convective velocity scale (w_*), but uses l_t instead of z_i. l_b is the length scale that primarily regulates the magnitude of the mixing lengths in stable conditions, in the mid- and upper convective boundary-layer and the free atmosphere as well. It not only regulates the strength of the vertical diffusion in the stable boundary layer but the entrainment between the boundary-layer and the free atmosphere as well (Lenderink and Holtslag 2000). The coefficient α_2 is important for modulating the size of l_b , and varies widely in the literature from

0.2 (Lenderink and Holtslag 2004) to 0.25 (Mahrt and Vickers 2003; they used σ_w/N) to 0.53 (Galperin et al. 1988; Furuichi et al. 2012) to 0.71 (Abdella and McFarlane 1997) to 1.0 (Nakanishi and Niino 2004 and 2009) to 1.69 (Nieuwstadt 1984; they also used σ_w/N). Not surprisingly, Lock and Mailhot (2006) suggest that the optimal value for α_2 may vary with boundary-layer regimes. This wide variety of values chosen for α_2 does, however, not necessarily reflect its range of uncertainty; rather, it can vary in different PBL schemes due to other compensating factors, such as choices of constants used to regulate the dissipation rate of TKE. Many values of α_2 have been tested within the MYNN and this parameter has been decreased in the WRF–ARW version of the MYNN from 1.0 to 0.65 to 0.3 in successive revisions of WRF–ARW.

The second term in the brackets of equation (11), hereafter termed the buoyancy enhancement term (BET), acts to enlarge l_b for conditions with a positive-surface heat flux ($\zeta < 0$), which helps to reduce the impact of l_b on the harmonically averaged mixing length when buoyancy effects should be minimized. This provides a mechanism for l_b to vary with boundary-layer regimes without needing to vary α_2. However, the dependence upon the surface heat flux in the BET is questionable since the surface fluxes may have little relevance to the turbulence well above the boundary layer. The exception would be in a deep convection regime, but mixing in this regime should be handled by a convection scheme and/or resolved convective plumes. The length scales, along with the harmonic averaging summarized above, represent the form found in the original MYNN and can be used within the current MYNN-EDMF when the namelist option *bl_mynn_mixlength* is set to 0.

ii. The first revision: *bl_mynn_mixlength* = 1

The first set of changes made to the mixing lengths were needed to solve three critical problems: (1) the excessively large magnitudes of l_t (mentioned above), (2) the dependency of l_b upon a local calculation of N can give rise to singularities in unstable layers and, since l_b is a function of l_t, which is only valid in the boundary layer, the original form of l_b should either only be used below z_i or the BET must be removed for use in the free atmosphere, (3) related to the changes in the stability functions (discussed in section 2.3), a reduction in mixing was required in stable conditions, and (4) a high 10-m wind speed bias was present during the daytime.

The first modification changed the limits of integration of l_t in (10). Instead of integrating from the surface to the top of the model atmosphere, it is now only integrated to the top of the PBL (denoted z_i), plus a transition layer (or entrainment layer) depth $\Delta z = 0.3 z_i$ (Garratt 1992). The original MYNN operated independently of z_i; that is, z_i was not used as an independent variable to diagnose other quantities within the scheme. This modification requires an accurate diagnostic calculation of z_i (described later in section 7.1).

An attempt to rectify the problems with l_b, was to implement a nonlocal mixing-length formulation from Bougeault and LaCarrere (1989; hereafter known as the "BouLac" mixing-length, l_{BL}). The algorithm for the BouLac involves looping upward and downward until vertical distances of displacement l_{up} and l_{down} are found which represent the distances a parcel can be displaced, given a local amount of TKE, within an ambient stratification. Then, an average of l_{up} and l_{down} is taken as $l_{BL} = (l_{up}^2 + l_{down}^2)^{1/2}$. Since this formulation is nonlocal in design, it is capable of diagnosing mixing lengths in unstable layers, such as breaking mountain waves, so it nicely addresses the

problems associated with (11). To restrict the use of l_{BL} to the free atmosphere and preserve the original MYNN mixing-length formulation in the boundary layer, a blending approach is adopted. A transition (or entrainment) layer is defined where the original buoyancy length scale, l_b, is used below z_i and l_{BL} is used above:

$$l_b = l_b(1 - W) + l_{BL}W \quad (12a)$$

$$W = 0.5tanh\left(\frac{z_i+\Delta z}{\Delta z/2}\right) + 0.5 \quad (12b)$$

This formulation makes the buoyancy-length scale equal to l_b below z_i, about 50% each at the top of the entrainment layer ($z_i + \Delta z$), and equal to l_{BL} above $z_i + 2\Delta z$. The specific depth of the layer used in this blending approach has little impact on the behavior of the turbulent mixing near the PBL top.

The final two modifications were simple tuning adjustments to counter other required changed or to reduced biases diagnosed in the RAP/HRRR. The first reduced the magnitude of the mixing in stable conditions, which was required after a change made to the closure constant A_2 to fix a negative TKE problem (described in section 2.3). This change, in consultation with Mikio Nakanishi, reduced the coefficient associated with l_b, α_2, from 1.0 to 0.65. A second modification reduced a high wind 10-m wind speed bias in the RAP/HRRR during the daytime. It was found that a reduction of α_4 from 100 to 20 sufficiently reduced l_s in unstable conditions, reducing the mixing of momentum down to the surface during the daytime.

This set of modifications completes the description of the first mixing-length revision to the MYNN and can be used by setting the namelist option *bl_mynn_mixlength* to 1. This version may still be optimal in many cases, especially without activating the mass-flux scheme *(bl_mynn_edmf* = 0).

iii. The second revision: *bl_mynn_mixlength* = 2

A second revision to the mixing lengths was attempted for the following reasons: (1) to devise a formulation that better complements the additional mass-flux component (described in section 3) by focusing on improved performance in stable boundary layers, (2) to gain more control of the magnitude of the averaged (or blended) mixing length, and (3) to improve computational efficiency. This last objective to reduce the computational expense resulted in a replacement of the BouLac that was added in the first mixing-length revision (*bl_mynn_mixlength* = 1).

The EDMF approach allows for some of the turbulent transport of heat, moisture, and momentum to be performed by mass-flux scheme in convective conditions, requiring less of the turbulent mixing to be performed by the eddy-diffusivity component. This allows us to configure the eddy-diffusivity (specifically the mixing lengths) portion of the MYNN-EDMF to specialize on treating the stable boundary layer, while the mass-flux component helps to carry the load in unstable conditions. The first modification was made to further reduce α_4 from 20 to 10, in an attempt to reduce the local mixing of momentum down to the surface, since the mass-flux scheme added additional mixing when activated. This had a small impact overall, but helped to maintain a near-zero, 10-m wind speed bias during the daytime in the RAP/HRRR with the mass-flux scheme activated. A second modification was made to α_2, further reducing it from 0.65 to 0.3. This effectively improved the maintenance of mountain valley cold pools and stable layers in regions outside of complex terrain. A final modification was made to improve the coupling of the mass-

flux scheme and the mixing lengths. The buoyancy length scale l_b was changed to $l_b = \alpha_2 \times \mathrm{MAX}(q, M)/N$, where M is the mass-flux (= total area of plumes × mean velocity of plumes; described in section 3) at a given model level. The impact of this modification is very small because q typically exceeds M.

The second modification was focused on obtaining more control of the magnitude of the mixing lengths. The harmonic averaging can result in dramatically reduced mixing lengths, less than 50% in magnitude of the smallest component (Figure 2). Alternative blending techniques were investigated.

The problem of the small-biased averaged mixing length was alleviated by reducing the number of components used in the harmonic average to two, using only l_s and l_t, as was proposed by Blackadar (1962), but included a MIN function to account for the effects of buoyancy represented by l_b:

$$l = MIN\left[\frac{1}{\frac{1}{l_s}+\frac{1}{l_t}}, l_b\right]. \qquad (13)$$

This method was originally proposed by Mikio Nakanishi (personal communication). This form makes the mixing length formulation more z-less in nature (Nieuwstadt 1984, Ha and Marht 2001)

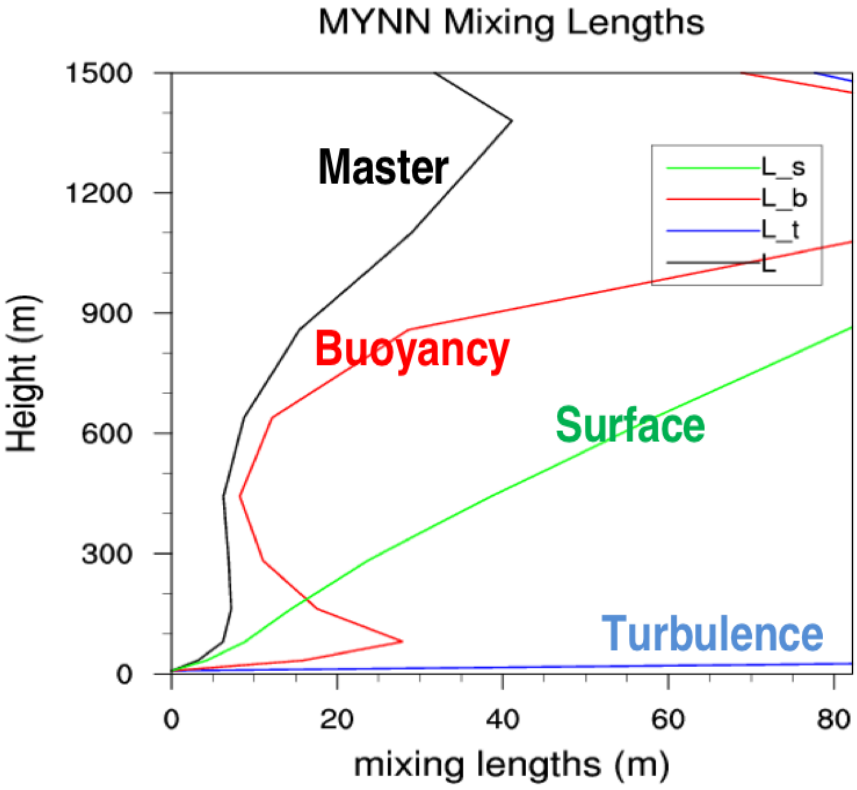

Figure 2. Example of each mixing length component (colors) and the harmonically averaged mixing length (black) for a stable situation below 500 m AGL.

when the buoyancy effects become the turbulence-limiting factor (l_b becomes the smallest length scale). In this situation, l_s and l_t do not impact l; only the local stability and turbulence (l_b) controls l.

The overall impact on maintaining the magnitude of the smallest specified length scale is shown in figure 3 for both a stable and unstable situation. The overall magnitudes of the revised length scale are similar near the surface but the revised l can be larger than the control (revision #1) due to the small-biasing of the three-variable harmonic averaging; however, due to the reduction of α_2, the revised l is typically smaller in the upper PBL and aloft. The difference between the smallest length scale and the blended l is mostly zero with the revised l, with the exception of the heights between 70 and 300 m AGL, where the harmonic averaging of two variables still results in an underestimation of 20–30% relative to the smallest length scale, but that is much smaller than the 50–65% underestimation by the original method. This new blending method gives more control of the magnitude of the blended mixing lengths, better matching the specification of the smallest individual mixing length scales, which can now be used more precisely to regulate the behavior of turbulent mixing in the MYNN-EDMF.

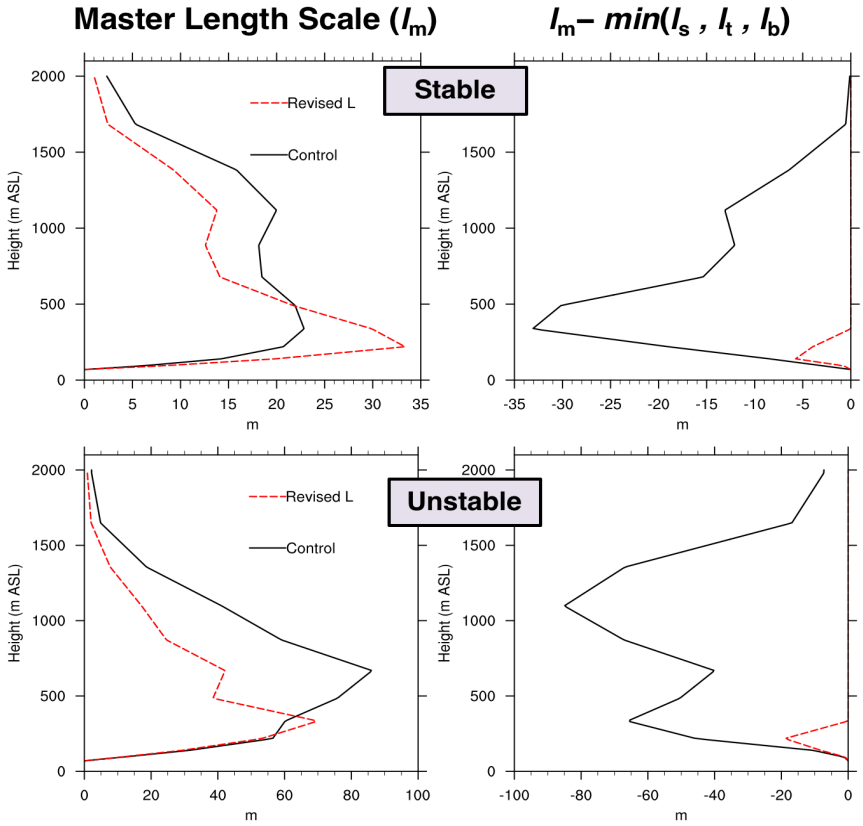

Figure 3. Example of mixing lengths for stable (top) and unstable (bottom) cases. The left side shows the magnitude of the mixing lengths for revision #2 compared to revision #1 (control). The right side shows the difference between the blended mixing length (l) and the smallest of the individual components.

Improvements to the computational efficiency of the mixing length required replacing the BouLac with an alternate length scale that is not prone to singularities in unstable layers. The cloud-specific length scale of Teixeira and Cheinet (2004) was chosen to replace the BouLac:

$$l_b = \tau(TKE)^{1/2} . \quad (14)$$

In the convective boundary layer, Deardorff (1970) suggests that the time scale τ is proportional to z_i/w_*, where z_i is the PBL height and w_* is the convective velocity scale:

$$\tau = 0.5 \frac{z_i}{(\frac{g}{\theta_0} z_i \overline{w'\theta'})^{1/3}} . \quad (15)$$

Above z_i, τ is set to 50 s. This TKE-based form is used in place of the original l_b (Eq. 11) in neutral or unstable layers, when N becomes non-positive.

Lastly, after all length scales are computed and blended into a vertical profile, another scale-adaptive blending function is applied to the mixing lengths to ensure that a relevant form is used for any particular model configuration within the boundary layer grey zone (2000 m > Δx > 200 m). This idea is taken from Cuxart et al. (2000) and Ito et al. (2015), where a "mesoscale" form of mixing lengths (as described above) is blended with a form more appropriate for LES. The

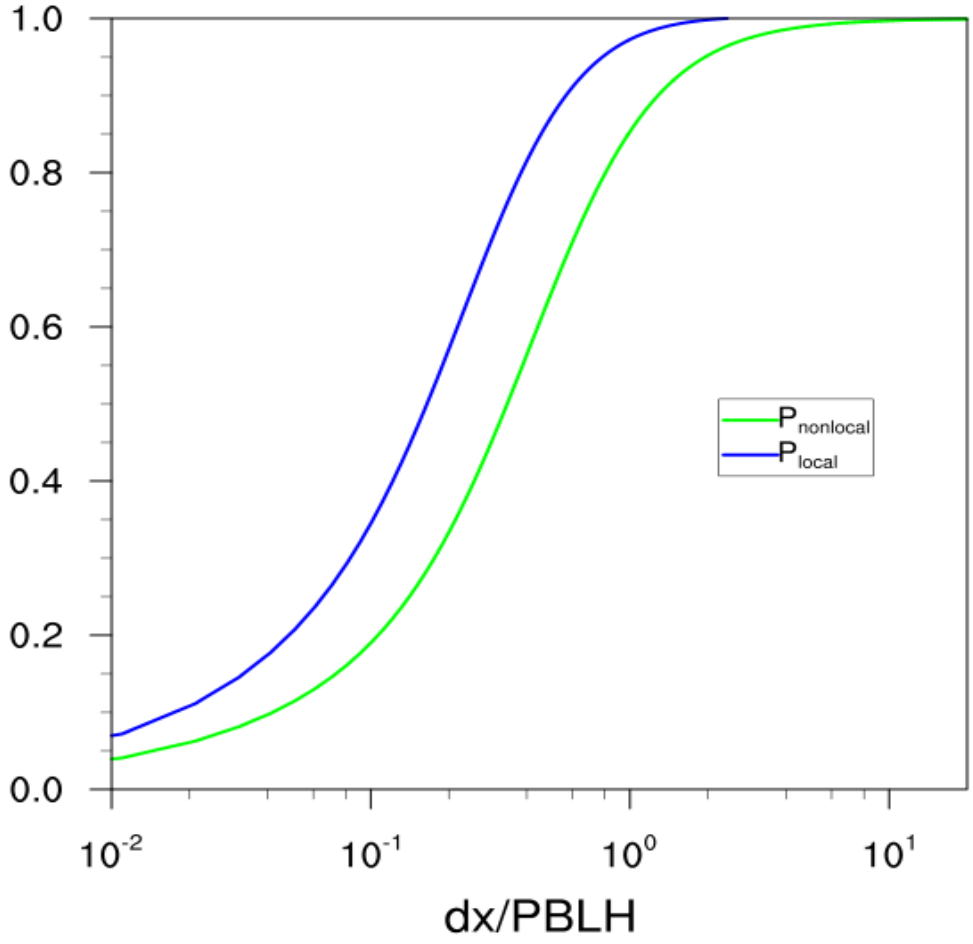

Figure 4. Tapering functions used for nonlocal processes (green) and local processes (blue). The local function is taken from Honnert et al. (2011), representing the variation of parameterized TKE in the boundary layer. The nonlocal function is taken from Shin and Hong (2013), and it represents the variation of parameterized TKE in the entrainment zone.

similarity functions P from Honnert et al. (2001) and Shin and Hong (2013) are used to perform this blending (Figure 4). The LES mixing length l_{LES} is a minimum of l_{b} and asymptotic form of ls to l_{∞} with height:

$$l = MIN\left[\frac{l_s}{1+\frac{l_s}{l_\infty}}, l_b\right], \tag{16a}$$

$$l = l_{meso}P + l_{LES}(1-P) \tag{16b}$$

Where l_{∞} is set to 15 meters, which is similar to that found observationally by Sun (2011) and Kim and Mahrt (1992). This makes the eddy-diffusivity component of the MYNN-EDMF *partially scale-adaptive* with respect to the model grid spacing. The authors would argue that to fully achieve scale-adaptive functionality, the 1-D mixing scheme should also transform to a 3-D mixing scheme like that used in LES configurations (Kurowski and Teixeira 2018), but this is beyond the scope of current operational forecasting needs.

2.3 Stability Functions

In the Mellor-Yamada framework, the level 2 stability functions S_H and S_M, are functions of the gradient Richardson number Ri, and the closure constants, which have been tuned to best match LES results in Nakanishi and Niino (2004 and 2009). All of the closure constants in the updated MYNN-EDMF remain the same, with the exceptions of A_2, C_2, and C_3. Kitamura (2010) introduced a simple modification to the MYNN based on the method proposed by Canuto et al. (2008). This modification applies a stability-dependent relaxation to the closure constant A_2, such that it becomes a closure *variable* in statically stable conditions (Ri > 0):

$$A_2 = \frac{A_2}{1+\max(Ri,0.0)} \tag{17}$$

In both the original MYNN and the MYNN-EDMF, the mixing length for vertical heat transport is given as $A_2 l$ (where l is the mixing length). Hence, this reformulation of A_2 causes the mixing lengths used for the turbulent heat flux to decrease with stronger static stability but does not affect the turbulent mixing of momentum. This modification was shown by Kitamura (2010) to remove the critical Richardson number ($\mathrm{Ri_c}$), allowing small finite momentum mixing to exist at Ri $\rightarrow\infty$, (Fig. 5) as argued for by various turbulence researchers (i.e., Galperin et al. 2007; Zilitinkevich et al. 2007; Canuto et al. 2008). This modification does not transform the MYNN into a total turbulent energy (TTE) scheme, like Mauritsen et al. (2007), Zilitinkevich et al. (2007), and Angevine et al. (2010), but does place the modified MYNN-EDMF into the same class of schemes that do not have a critical Ri.

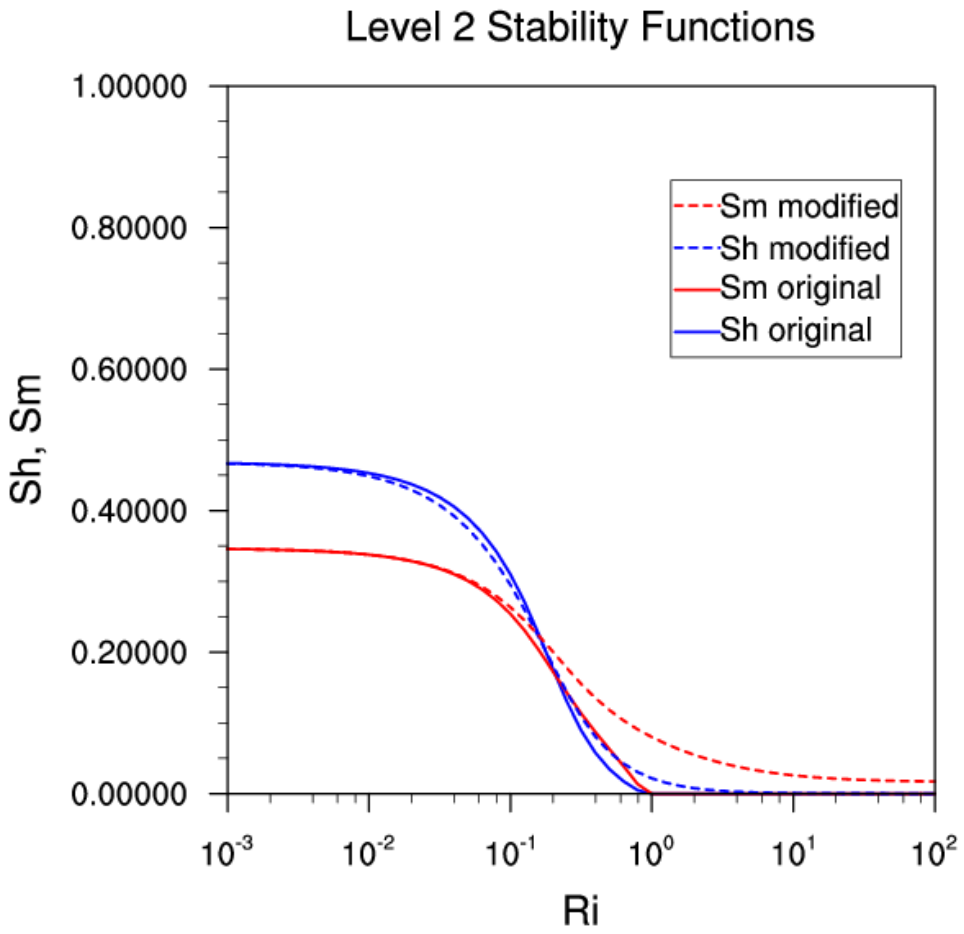

Figure 5. Original (solid) and modified (dashed) Level 2 stability functions for momentum (red) and heat (blue).

Kitamura (2010) cautioned that this modification may require subsequent adjustments to reduce the closure constants C_2 and C_3. After consulting with Mikio Nakanishi, we revised C_2 and C_3 to 0.729 and 0.34, respectively, which fall within the range suggested by Gambo (1978); however, test simulations revealed that the removal of Ri_c resulted in increased mixing in stable conditions, spurring efforts to further reduce the mixing-length scales in stable conditions as described above. This modification has existed in the MYNN in WRF–ARW since approximately v3.7 and is activated by default.

3. Dynamic Multiplume Mass-Flux Scheme

Eddy-diffusivity schemes perform reasonably well in stable boundary layer applications, but cannot adequately describe the nonlocally-driven turbulent fluxes in the upper part of the convective boundary layer or represent the clouds produced by convective plumes. Additional nonlocal components must be added to eddy-diffusivity schemes, such as counter-gradient terms or explicit entrainment parameterizations, to represent the nonlocal mixing. The original MYNN

PBL scheme has some representation of nonlocal mixing when run at level 3, which makes use of counter-gradient flux terms; however, the level 2.5 model is primarily a local-mixing scheme (when not considering nonlocal aspects of the mixing length formulation, discussed in section 2).

A more sophisticated approach for the representation of nonlocal mixing in convective boundary layers is the mass-flux method. Siebesma et al. (2006) have shown that this approach has strong advantages over the more traditional counter-gradient approach, especially in the entrainment layer. Mass-flux schemes can represent the nonlocal turbulent transport by thermal plumes for both dry and cloud-topped boundary layers. Boundary layer thermals or plumes can be thought of as the invisible roots that produce shallow cumulus clouds (Lemone and Pennell 1976). Therefore, mass-flux schemes provide a way to represent these plumes and allow for a direct coupling of subcloud convective cores with the cloud layer above. The inclusion of a mass-flux scheme within the MYNN PBL scheme moves it into the class of eddy-diffusivity mass-flux (EDMF) schemes as well as the category of nonlocal mixing schemes.

The MYNN-EDMF is used within RAP and HRRR forecast systems, which are responsible for providing a wide range of forecast guidance, such as the timing and location of severe convection, cloud ceilings, precipitation, and low-level winds, so improvements to the representation of strong thermals in the convective boundary layer must not come at the expense of these other metrics. Specific design features are added to the mass-flux scheme to help generalize its applicability to any relevant weather regimes. Furthermore, since the RAP/HRRR physics suite is often used for much higher resolution (subkilometric) applications in support of major field studies, the mass-flux scheme must be designed to perform well at moderate to small horizontal grid spacing (5 km to 750 m), which spans the grey zone of shallow-convection modeling. This requires the integration of scale-adaptive flexibility into a state-of-the-science, mass-flux parameterization, such as the designs of Neggers (2015) and Sušelj et al. (2013), which inspired the design of this scheme. The following subsections describe the overall design, scale-adaptive features, and configuration options for the MYNN-EDMF.

The blending of the mass-flux scheme with the eddy-diffusivity scheme requires a partitioning of the total turbulent fluxes, such that the vertically coherent convective updrafts represented by the mass-flux scheme cover a fraction of the model grid cell, a_u, and the rest of the grid cell, 1-a_u, contains the small-eddy mixing associated with the eddy-diffusivity scheme. We will formally define a_u later. With this approximation, the total turbulent fluxes (mixing and transport) of any arbitrary variable $\boldsymbol{\phi}$ can be represented as three terms following Siebesma and Cuijpers (1995):

$$\overline{w'\phi'} = a_u\overline{w'\phi'}^u + (1-a_u)\overline{w'\phi'}^e + a_u(w_u - \bar{w})(\phi_u - \phi_e) \qquad (18)$$

where the sub- and superscripts u and e refer to the area of convective updrafts and environment, respectively. For the rest of this description, we ignored the sub- and superscripts e and assumed that all unscripted variables describe the environment or model grid cell mean. The first term on the rhs of (18) is typically neglected with the assumption that $a_u \ll 1$. The second term represents the small-eddy mixing in the nonconvective plume portion of the grid cell, which is represented by the eddy-diffusivity scheme. The third term of the rhs of (18) represents the nonlocal turbulent transport from the convective mass flux, defined as $M \equiv a_u(w_u - w)$. This term can replace the counter-gradient term, γ, in equation (1), which can now be approximated as:

$$\overline{w'\phi'} \cong -K_{h,m}\frac{\partial \phi}{\partial z} + M(\phi_u - \phi). \quad (19)$$

In the MYNN-EDMF, the second term in (19) is represented with a multiplume approach, following Neggers (2015) and Sušelj et al. (2013), so summation notation is more appropriate:

$$\overline{w'\phi'} \cong -K_{h,m}\frac{\partial \phi}{\partial z} + \sum_{i=1}^{n} M_i(\phi_{u_i} - \phi)\,, \quad (20)$$

where i represents an individual plume and n is the total number of plumes. Like the eddy-diffusivity parameterization, which is meant to represent an ensemble of turbulent eddies of various sizes, the approach of Neggers (2015) attempts to represent a variety of convective plumes of various sizes. We adopt this approach here, where a maximum number of 10 plumes are available for activation within a model grid column, representing plume diameters d = 100, 200, 300, …, and 1000 m. Each plume can be dry or, if extending above the lifting condensation level (LCL), can condense and produce shallow cumulus clouds. The only distinguishing aspect to each plume is the entrainment rate ε_i, which is taken from Tian and Kuang (2016):

$$\varepsilon_i = \frac{\varepsilon}{w_i d_i} \quad (21)$$

where w_i is the vertical velocity and d_i is the diameter of each plume i. The constant c_ε is set to 0.35, which is larger than the value (0.23) estimated by Tian and Kuang (2016) in LES experiments. In their study, they defined d as the distance to the edge of the cloud as opposed to the plume diameter, so a slightly larger value better fits our definition of d. This diameter-dependent entrainment rate allows each plume to evolve differently; thus, attempting to represent a broad range of thermals in a convective boundary layer.

Although the total number of plumes available for activation is 10, not all meteorological conditions are associated with large plumes. A good example is midmorning, when the surface heat fluxes become positive (directed upward) but the boundary layer is still only beginning to build. In this condition, no 1000-m plumes are yet formed; rather, the largest plumes approximately scale to the depth of the subcloud-layer height (Neggers et al. 2003). Here we approximated the maximum plume width to scale with the boundary layer height, z_i, up to z_i = 1000 m. An additional limitation on the maximum plume width is exercised in the case where there exists a cloud ceiling, defined as a model layer with cloud fraction in excess of 50%, in the lowest 2000 m of the atmosphere. In this case, the maximum plume width is set to $z_c/2$, where z_c is the ceiling height. This allows the number of available plumes to dynamically evolve with the growing/collapsing boundary layer and/or with cloud depth, making the MYNN-EDMF s*cale-adaptive with respect to the relevant scales of the meteorological conditions*. A final limitation to the maximum number (or size) of plumes is related to the horizontal grid spacing, Δx, in meters. We imposed a limit on the maximum plume width to be less than Δx, so there is no attempt to parameterize plumes greater

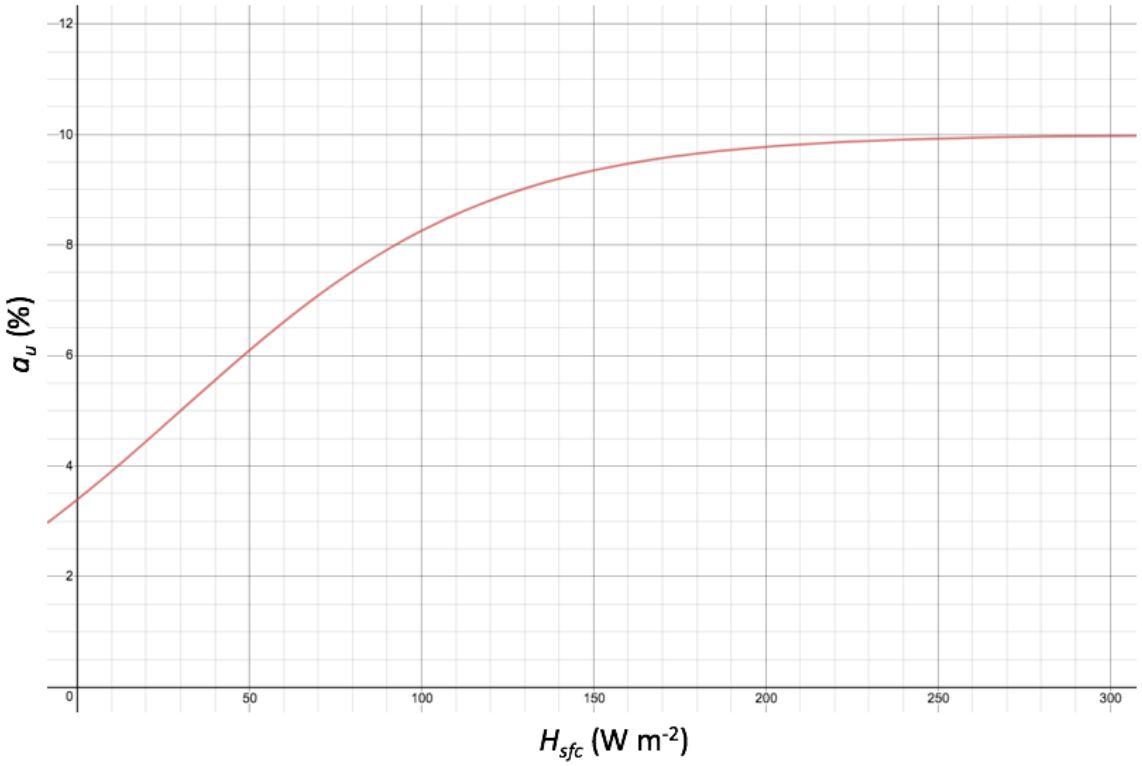

Figure 6. Function to regulate the fractional areal coverage (a_u, %) of the convective plumes within a model grid column as a function of the surface buoyancy flux (H_{sfc}, W m-2) described by equation (22).

than or equal to what can be resolved. This makes the MYNN-EDMF *scale-adaptive with respect to the model grid spacing*. Each of these conditions are checked at every model time step, dynamically regulating the number of plumes available for activation within each model grid column.

The activation criteria of the mass-flux scheme in the MYNN-EDMF is threefold, where all three conditions must be met. (1) The conditions above that determine the maximum number (or largest size) of plumes to be activated must specify at least one plume is to be used; (2) there must be a positive surface buoyancy flux; (3) the model surface layer must be superadiabatic in the lowest 50 m. If any one of these conditions fail, then the mass-flux scheme will be inactive and the MYNN-EDMF is run in eddy-diffusivity configuration only for that model grid column at that specific time step.

If the activation criteria are met, the next step is to calculate the total updraft area a_u, implying the area of vertically coherent plumes only - not the area of all turbulent eddies. Many EDMF schemes use a constant a_u, varying from of 0.04 (Sušelj et al. 2013) to 0.05 (Kohler et al. 2011) to 0.1 (Soares et al. 2004; Neggers et al. 2009; Witek et al. 2011) or can vary with height (Angevine et al. 2010). The MYNN-EDMF also uses a constant a_u with height for each plume, but a_u is made a function of the surface buoyancy flux, H_{sfc}. The purpose is to act as a "soft triggering" mechanism, as discussed in Neggers et al. (2009), allowing the mass-flux scheme to vary in strength more continuously as opposed to abrupt activations/deactivations. We used a hyperbolic tangent

function (Fig. 6)

$$a_u = a_{max}\left[\frac{1}{2}\tanh\left(\frac{H_{sfc}-20}{90}\right)+\frac{1}{2}\right], \quad (22)$$

so a_u is near a_{max} (=10%) for H_{sfc} > 200 W m^{-2} but can be as small as 33% for H_{sfc} near 0 W m^{-2}. We considered this exact form to be uncertain, so we are still investigating it.

Once the number of plumes N and the total updraft area a_u is known, a_u must be divided appropriately among the N plumes. That is, the turbulent transport contributed by each plume is mapped to a portion of a_u by way of the power law, which relates the number density, $\mathcal{N}$, of each plume size to the plume size following Neggers (2015):

$$\mathcal{N}(d) = Cd^x\,, \quad (23)$$

where d is the plume diameter, C is a constant of proportionality, and x is the power law exponent, set to -1.9, same as Neggers (2015). This power law effectively weights the contributions of each of the various plumes to the total convective transport in the model grid column. With x=-2, each of the plumes covers an identical portion of a_u, but with x > -2, the largest plumes have a slightly larger contribution than the smallest plumes. We set x = -1.9, same as Neggers (20015), which is based off of a combination of observations and LES (Benner and Curry 1998, Neggers et al. 2003, Yuan 2011). With a dynamic number of plumes, C must be solved for and normalized such that the total area of n plumes covers a_u (defined above). This departs from Neggers (2015) in that we did not assume all 10 plumes, representing widths from 100 to 1000 m, are active within a given grid cell and a_u is not constant in time, but the power law weighting is the same. Neggers (2015) planned to relax these constraints in future research.

With the number of plumes n, the total updraft area a_u, and the individual plume areas determined, the initialization and integration of the plumes can commence. Each of the updrafts are initialized at the top of the first model layer with vertical velocities:

$$w_{u_i} = p_w\sigma_w\,, \quad (24)$$

where p_w varies from 0.1 to 0.5 between the smallest and largest plumes and σ_w is defined further below. The initialized w_u is not allowed to exceed 0.5 m s^{-1}. The initial plume properties for temperature and moisture are averages of the first and second model layers, representing a value at the interface between the first and second model layers. We assumed that the averaged quantities were slightly boosted with a thermal and moisture excess defined as:

$$\theta_{li_{u_i}} = \theta_{li} + w_{u_i}C_{w\theta}\frac{\sigma_\theta}{\sigma_w}, \text{ and} \quad (25)$$

$$q_{t_{u_i}} = q_t + w_{u_i}C_{w\theta}\frac{\sigma_{q_t}}{\sigma_w}. \quad (26)$$

The constant $C_{w\theta}$ = 0.58 (Sorbjan 1991) and the standard deviations of w, q_t and θ were specified as:

$$\sigma_w = C_\sigma w_*(z_s/z_i)^{1/3}(1-0.8z_s/z_i) \quad (27a)$$

$$\sigma_{qt} = C_\sigma q_*(z_s/z_i)^{-1/3} \quad (27b)$$

$$\sigma_\theta = C_\sigma \theta_*(z_s/z_i)^{-1/3} \quad (27c)$$

where C_σ = 1.34, z_s=50 m, w_* is the convective velocity, q_* is the surface moisture flux divided by

w_* (kg kg^{-1}), and θ_* is the surface temperature flux divided by w_* (K). The above similarity expressions used to specify the excess heat and moisture were verified from observational studies over land (i.e., Wyngaard et al. 1971). For more details, see Cheinet (2003). We noted that the excess quantities added to the parcel initializations only have a secondary impact on the evolution of the plumes. As found in other studies (Brast et al. 2016), the primary factors determining the fate of rising thermals is the entrainment rates and the background stability within the model grid column.

We designed the MYNN-EDMF to transport momentum and TKE, but these quantities are not transported by default in WRF–ARWv4.0. WRF namelist options, *bl_mynn_edmf_mom* and *bl_mynn_edmf_tke*, must be set to 1 to activate momentum and TKE transport, respectively (refer to Appendix). When activated, the plume horizontal velocity components, *u* and *v*, are initialized by averaging *u* and *v* between the first and second model layers. We used the same averaging to initialize TKE. We did not add any additional excess quantities to these mean velocity components and TKE.

The vertical integration of each plume is performed with an entraining bulk plume model for the variables $\varphi = \{\theta_{li}, q_t, u, v,$ and TKE$\}$. As in Teixeira and Siebesma (2000) and most other mass-flux schemes, we used a simple entraining rising parcel:

$$\frac{\partial \phi_{u_i}}{\partial z} = -\varepsilon_i(\phi_{u_i} - \phi) \tag{28}$$

where ε_i is the fractional entrainment rate, defined above, which regulates the lateral mixing of the updraft properties, φ_{ui}, with the surrounding air, φ.

The vertical velocity equation using a modified version of that from Simpson and Wiggert (1969), with the buoyancy $B = g(\theta_{v,ui} - \theta_v)/\theta_v$ as a source term:

$$w_{u_i}\frac{\partial w_{u_i}}{\partial z} = -\varepsilon_i a w_{u_i}^2 - bB \tag{29}$$

The coefficients *a* and *b* are discussed in several papers (e.g. Siebesma et al. 2003; de Roode et al. 2012). They represent the effect of pressure perturbations and subplume turbulence terms. The precise value of these coefficients is still a subject of research and diagnosed values from LES studies give different results in the cloud layer and in the subcloud layer . Here $a = 2.0$. The impact of buoyancy is governed by *b*, which takes the value 0.15 when the buoyancy *B* is positive and 0.2 when *B* is negative. Some limits are in place to prevent unreasonably large values of *w* from developing, such as a maximum layer depth of $\Delta z = 250$ m and a maximum updraft vertical velocity of $w_{ui} = 3$ m s^{-1}.

To summarize the plume integration procedure, at each model level, the following steps are performed for each of the *n* plumes: (1) the entrainment rates are determined; (2) the plume variables are solved for using Eq. (28); (3) then the buoyancy term *B* and the vertical velocity equation (29) are solved. This is repeated at each model level until each plume terminates by reaching a height at which w_{ui} becomes ≤ 0. Then the mean convective mass-flux and plume properties are calculated by using the power-law weighting of each of the *n* plumes.

We added further scale-adaptive capability to limit the impact of the mass-flux scheme at the high-resolution end of the shallow-cumulus grey zone (1000 m > Δx > 200 m). Despite the features described above, which limit the plume sizes as the horizontal grid spacing decreases, we used the similarity functions *P* from Honnert et al. (2011) and Shin and Hong (2013) to perform the tapering

of a_u: $a_u = a_u * P$. This reduces the mass-flux contribution to total mixing in the MYNN-EDMF to less than 20% for grid spacing below $\Delta x = 500$ m. Further testing is needed to determine if this rate of tapering of the mass-flux contribution is optimal for model configurations in the middle of the shallow-cumulus grey zone.

Lastly, the linkage of the mass-flux transport to the creation of boundary-layer clouds is a primary incentive for adding the mass-flux component. As part of the integration process, at each model level, a saturation check is performed after calculating the plume thermodynamic state. If condensation occurs, latent heat is released, which directly impacts the parcel's buoyancy term in (28). This typically results in an acceleration of the parcel and an increased mass-flux M. For all condensed plumes, the determination of the cloud fraction and the contribution to the buoyancy production of TKE becomes an important additional step. We discuss this in the following section.

4. Subgrid Clouds and Buoyancy Flux

The representation of subgrid-scale (SGS) clouds and their connection to SGS turbulence is an important aspect in both general circulation and limited-area mesoscale models. This is typically accomplished by use of joint probability distribution functions, known as cloud probability distribution functions (cloud PDFs, also known as partial-condensation schemes), which can either make use of the higher-order moments or vertical gradients of the resolved-scale fields to determine the SGS cloud mixing ratio, cloud fraction, and the buoyancy flux. The more sophisticated forms (i.e., Golaz et al. 2002), which rely on additional prognostic equations, allow for a more direct physically consistent interaction between the higher-order turbulent quantities and the clouds, but come with a computational cost. The simpler forms, such as Sommeria and Deardorff (1977), Mellor (1977), and Chaboureau and Bechtold (2002 and 2005; hereafter CB02 and CB05, respectively) are generally capable of representing first-order macrophysical aspects of subgrid clouds and are effective at reducing time step variability in TKE-based schemes associated with grid-scale condensation. This is because the statistical representation of the SGS cloud properties evolve more continuously and consistently as the background moisture changes in the model grid cell (Sommeria and Deardorff 1977).

The original MYNN was designed with the representation of SGS clouds, using the cloud PDF from Sommeria and Deardorff (1977). In early versions of WRF–ARW (pre-v3.8), the macrophysical properties (SGS cloud fraction and SGS liquid water content) from this cloud PDF were only used to parameterize the SGS buoyancy flux; coupling to the radiation scheme was not yet performed. Since v3.8, more cloud PDFs have been integrated into the MYNN with full coupling to the radiation. Namelist parameters were added to WRF–ARW to switch between different cloud PDFs (i.e., *bl_mynn_cloudpdf*) and to active the coupling to the radiation scheme (i.e., *icloud_bl*) (refer to Appendix). We describe a description of each option for the namelist parameter *bl_mynn_cloudpdf* below. We describe *icloud_bl*, on the coupling to the radiation scheme in section 6.1.

4.1 Cloud PDF Options

i. Original (Gaussian) form: *bl_mynn_cloudpdf* = 0

The original cloud PDF described in Nakanishi and Niino (2004) is based on the joint-Gaussian probability distribution functions for the liquid potential temperature θ_l and total water content q_t proposed by Sommeria and Deardorff (1977) and Mellor (1977). We essentially repeat the description here for comparison to alternative approaches later. In this approach, the standard deviation is estimated using the second-order moments in the MYNN. The cloud water content q_l can be written as

$$q_l = 2\sigma_s \left[A_{cf} Q_1 + \frac{1}{\sqrt{2\pi}} exp\left(-\frac{Q_1^2}{2} \right) \right] \quad (30)$$

and the areal cloud fraction A_{cf} is:

$$A_{cf} = \frac{1}{2}\left[1 + erf\left(\frac{Q_1}{\sqrt{2}} \right) \right] \quad (31)$$

The normalized saturation deficit is:

$$Q_1 = \frac{a(q_t - q_{sat})}{2\sigma_s} \quad (32)$$

and the variance of the saturation deficit,

$$\sigma_s^2 = \frac{a^2}{4}(\langle q_t'^2 \rangle - 2b\langle \theta_l' q_t' \rangle + b^2 \langle \theta_l'^2 \rangle), \quad (33)$$

and a and b are thermodynamic functions arising from the linearization of the functions for the water vapor saturation mixing ratio:

$$a = \left(1 + \frac{L_v}{p} \delta Q_{sat} \right)^{-1}, b = \frac{T}{\theta} \delta Q_{sat}.$$

$Q_{sl} \equiv Q_s(T_l)$ and $\delta Q_{sl} \equiv \partial Q_s / \partial T_l$ are determined from the Tetens formula and the Clausius–Clapeyron equation, respectively, where Q_s is the saturation-specific humidity and $T_l = \theta_l T/\theta$, and L_v is the specific latent heat of vaporization.

The form of the buoyancy flux, $w'\theta_v'$, in the MYNN TKE equation is:

$$\langle w'\theta_v' \rangle = \beta_\theta \langle w'\theta_l' \rangle + \beta_q \langle w'\theta q_t' \rangle \quad (34)$$

Where the buoyancy functions are:

$$\beta_\theta = 1 + 0.61 q_t - 1.61 q_l - Rabc$$
$$\beta_q = 0.61\theta + Rac$$

and

$$R = A_{cf} - \frac{q_l}{2\sigma_s} \frac{1}{\sqrt{2\pi}} \exp\left(-\frac{Q_1^2}{2} \right)$$
$$c = (1 + 0.61 q_t - 1.61 q_l) \frac{\theta}{T} \frac{L_v}{p} - 1.61\theta \ .$$

ii. First-order form: *bl_mynn_cloudpdf* = 1,-1

When using the level 2.5 configuration of the MYNN, the higher order moments (with the exception of the TKE) are diagnostically calculated. Therefore, the higher-order moments may be less accurate, limiting their usefulness in the original cloud PDF. We then integrated into the MYNN an alternative form, which avoids the use of the higher-order moments. This form is based on Nakanishi and Niino (2004) and Kuwano-Yoshida et al. (2010). It uses a different expression for σ_s, based off of gradients of the first-order fields (θ_l and q_t),

$$\sigma_s = \sqrt{\frac{a^2 l^2 B_2 S_h}{4}\left(\frac{\partial q_t}{\partial z} - b\frac{\partial \theta_l}{\partial z}\right)^2}, \quad (35)$$

but is also dependent upon on the mixing lengths, L, a closure constant B_2, the stability function for heat S_H, and thermodynamic variables a and b (defined above). Kuwano-Yoshida et al. (2010) added a lower limit on $S_H = 0.03$, arguing that a minimum is necessary for coarse vertical resolution model configurations to compensate for under-resolved strength and variation of inversions. Therefore, this form is likely preferable to the original form for course-resolution modeling and possibly when run at level 2.5. The calculation of the buoyancy is the same as outlined above for *bl_mynn_cloudpdf* = 0.

Note that the negative option (*bl_mynn_cloudpdf* = -1) is for testing only. This option disables the "nonconvective" portion of the SGS clouds so simulations can be done with the convective SGS clouds from the mass-flux scheme only. This allows for a convenient way to test changes in the mass-flux scheme without the ambiguity of other sources of SGS clouds.

iii. Non-gaussian form: *bl_mynn_cloudpdf* = 2,-2

CB02 introduced a statistical SGS cloud scheme for representing nonconvective, or stratus, clouds. As in Sommeria and Deardorff (1977), the cloud fraction and diagnosed cloud water are functionally dependent on a single variable, the normalized grid box saturation deficit Q_1, but CB also uses a form for σ_s based off of gradients of the first-order fields. The subgrid variability of the saturation deficit, σ_s, is expressed as:

$$\sigma_{s-strat} = c_\sigma l\left(a^2\frac{\partial q_t}{\partial z} - \frac{2ab}{pm}\frac{\partial h_l}{\partial z}\frac{\partial q_t}{\partial z} + \frac{b^2}{\frac{2}{pm}}\left(\frac{\partial h_l}{\partial z}\right)^2\right)^{1/2} \quad (36)$$

where h_l is the grid box mean moist static energy and l is the mixing length from the turbulence scheme (described in section 2.2). In this manner, the diagnosed cloud fraction and cloud water amounts are directly linked to the amount of simulated turbulence. However, CB02 set l to a constant value of 900 m and was later revised in CB05 to l = 620 m. The parameter c_σ is a tuning constant, originally set to 0.2, and a and b are thermodynamic functions (defined above). c_{pm} is the heat capacity of moist air (= $c_{pd} + q_t c_{pv}$). In a nonconvective boundary layer, this estimate of the subgrid scale variation of saturation state appears sufficient to accurately simulate the evolution of nonconvective SGS clouds, but to account for convective clouds, we extended this scheme by CB05.

The standard deviation of the subgrid saturation deficit is proportional to the mass flux, M:

$$\sigma_{s-conv} \approx \alpha_{conv} M a^{-1} \quad (37)$$

where α_{conv} is a constant of proportionality (≈5E-3) and a^{-1} is used as a vertical scaling function (a is defined above). With both the stratus and convective component of σ_s defined, CB05 then redefined $\sigma_{s\text{-conv}}$ to be:

$$\sigma_{s-conv} = \sqrt{\sigma_{s-strat}^2 + \sigma_{s-conv}^2}. \quad (38)$$

The new $\sigma_{s\text{-conv}}$ is then used to calculate the normalized saturation deficit using (32), which is then used to calculate the SGS areal cloud fraction:

$$A_{cf} = max\left\{0, min\left[1, \frac{1}{2} + 0.36\text{atan}\,(1.55Q_1)\right]\right\}. \quad (39)$$

Note that we use this same equation for A_{cf} for the SGS stratus component, but only $\sigma_{s\text{-}strat}$ is used to calculate Q_1 using (32).

We included the following modifications to CB02 and CB05: (1) a factor of m [= 1 + MAX(RH-RH_c, 0)/(RH_{ss}-RH_c), where RH is the relative humidity, RH_c = 0.83 and RH_{ss} = 1.01] multiplied by A_{cf} for nonconvective cloud component only, allowing A_{cf} to exceed 50% in high relative humidity (stratus) conditions, (2) the tuning constant c_σ was increased to 0.225, (3) the mixing length l in the boundary layer was amplified in convective conditions with strong surface heat fluxes, such that l can be increased up to 600 m, but is otherwise relaxed to 300 m in nonconvective conditions and above the boundary layer, and (4) the tunable constant α_{conv} in the mass-flux portion of σ_s, $\sigma_{s\text{-}conv}$, is set to α_{conv} = 0.009. With the exception of (3), these modifications slightly increase the cloud fractions relative to CB02 and CB05.

As noted above, we use the negative option (*bl_mynn_cloudpdf* = -2) for testing purposes only. This option disables the "nonconvective" portion of the SGS clouds so simulations can be performed with the convective SGS clouds (from the mass-flux scheme) only. This allows for a convenient way to isolate testing to the mass-flux clouds without the ambiguity of other sources of SGS clouds.

4.2 Temporal Dissipation of Subgrid Cloud Fraction

The SGS shallow-cumulus clouds produced by the MYNN-EDMF will vary from time step to time step as the ambient environment and its forcing change. However, in nature, forced shallow-cumuli can persist in a passive phase well after genesis. To retain some SGS cloud fraction information at subsequent time steps, we implemented a temporal dissipation as:

$$A_{cf}{}^{t+\Delta t} \geq A_{cf}{}^{t} - A_M \frac{\Delta t}{\Delta t_{diss}}. \qquad (40)$$

Thus, the cloud fraction is only allowed to dissipate by $A_M(\Delta t/\Delta t_{diss})$ in one time step. If the current predicted cloud fraction at time $t+\Delta t$, $A_{cf}{}^{t+\Delta t}$ is greater than the dissipated cloud fraction from the previous time step, $A_{cf}{}^{t} - A_M(\Delta t/\Delta t_{diss})$, then we use the current predicted cloud fraction. The factor A_m = 0.25 corresponds to typical shallow-cumulus cloud fraction, and we set Δt_{diss} equal to the eddy turnover time scale, Δt_{eddy} = 1800 s. This time scale is adequate for low to moderate wind speed regimes or at coarse model grid spacing, but a higher rate of dissipation is needed at high horizontal resolution with moderate-high background wind speeds. In these conditions, the SGS clouds may inappropriately linger within a grid cell for a longer time than it would take to advect a parcel through the grid cell. Therefore, the timescale of dissipation is further restricted by the advective time scale, $\Delta t_{adv} = 3\Delta x/U$, where Δx is the model horizontal grid spacing and U is the resolved mean horizontal wind speed in the model grid cell. We set Δt_{diss} to the minimum of Δt_{eddy} and Δt_{adv}. This feature has a relatively small impact, but overall, acts to slightly smooth out the SGS cloud field.

5. Solution of the EDMF Equations

We solve the equations for turbulent diffusion/transport simultaneously for eddy-diffusion and mass-fluxes using a semi-implicit method. The code work performed for this integration of the mass-flux scheme with the eddy-diffusivity tridiagonal solver was originally performed by Kay

Sušelj (NASA-JPL). The discretization follows that which was proposed by Teixeira and Siebesma (2000) and Siebesma et al. (2007):

$$\frac{\phi^{t+\Delta t}-\phi^{t}}{\Delta t} = \frac{\partial}{\partial z}\left(K_{\phi}^{t}\frac{\partial \phi^{t+\Delta t}}{\partial z}\right) - \frac{\partial}{\partial z}\left[M^{t}(\phi_{u}^{t} - \phi^{t+\Delta t})\right] + S_{\phi}^{t} \qquad (41)$$

The generic variable ϕ on the rhs is solved implicitly, but the ED and MF coefficients and the updraft fields are taken explicitly. S_{ϕ} is a source term, which can be surface-based or elevated. In the case of the mass-flux plume sources, plume properties at interface levels k+½ and k-½ are differenced to determine a source at center of layer k. All equations are solved on a staggered grid with the scalars and winds being defined on the middle of the model layers and the turbulence variables ($K_{H,M}$ and M) on model layer interfaces. Linear interpolation between levels is performed to transform TKE from mass levels to model interfaces in order to compute $K_{H,M}$. For the space discretization, centered differences in space are used for the diffusion term and a simple first-order upwind scheme is used for the mass-flux integration. At the lowest model level, equation (41) is modified to include the surface fluxes, which are input from either a land-surface model or surface layer scheme at water grid points. At the top of the atmosphere, the turbulent fluxes are set to zero. The tridiagonal matrix equation is solved by a downward elimination scan followed by back substitution in an upward scan (Press et al. 1992, pp. 42–43).

To safeguard against pathological behavior, the combined heat flux from all plumes between the first and second model levels is forced to be less than 75% of the upward surface heat flux. Enforcing this will result in a modification of the total area of the updrafts throughout the depth of the penetrating plumes. This does not impose a strict limitation on the behavior of the mass-flux scheme, since this criteria is typically violated less than 2% of the time.

6. Communication with Other Model Components

6.1 Radiation Scheme

The SGS clouds produced by the MYNN-EDMF (section 3) are coupled to the longwave and shortwave radiation schemes if the namelist parameter *icloud_bl* is set to 1. In this case, the SGS cloud fraction, *CLDFRA_BL*, and the SGS cloud-mixing ratio, *QC_BL*, are added to the microphysics arrays within the radiation driver. The following two steps are performed: (1) the cloud fraction of the resolved-scale clouds are computed, using Xu and Randal (1996b) by default; (2) if the resolved-scale cloud liquid and ice, q_c and q_i, is less than 10^{-6} kg kg^{-1} and 10^{-8} kg kg^{-1}, respectively, and there exists a nonzero SGS cloud fraction, then the SGS components are added to their respective resolved-scale components by a temperature weighting, according to a linear approximation of Hobbs et al. (1974):

$$W_{ice} = 1 - MIN(1, MAX(0, (T - 254)/15))$$
$$W_{h2o} = 1 - W_{ice}$$

Then we sort the SGS cloud water and liquid as:

$$q_c = QC\_BL * W_{h2o} * CLDFRA\_BL$$
$$q_i = QC\_BL * W_{ice} * CLDFRA\_BL.$$

This allows us to only use one 3-D array for both SGS cloud water and ice. The updated q_c, q_i, and *CLDFRA* are then used as input into the radiation schemes. After exiting the radiation schemes, the original values of q_c, q_i, and *CLDFRA* are restored, so the SGS clouds do not impact the resolved-scale moisture budget.

6.2 Surface-Layer and Land-Surface Model

In WRF–ARW, the MYNN surface-layer scheme (not described in this document) is called prior to the call to the Land-Surface Model (LSM), which is called prior to the PBL schemes. The MYNN surface-layer scheme computes the surface stability parameter *z/L*, transfer coefficients, and the momentum and scalar fluxes (u_*, HFX, and QFX) over land, water, and snow grid points; however, the LSM will recalculate the scalar fluxes over land and snow grid points (assuming WRF is configured to use an LSM). The MYNN-EDMF uses the following as input: u_*, HFX, QFX, and *z/L*. The first three variables are used for a variety of calculations, such as lower-boundary conditions for the solver or initializing the parcels for the mass-flux scheme. The surface stability parameter *z/L* is used for computing the surface-layer length scale.

6.3 Microphysics Scheme (Thompson-centric)

WRF–ARW splits the moisture species into a defined set of "moist" and "scalar" arrays. The MYNN-EDMF scheme can mix either type, but it must be handled differently. For example, in WRF–ARWv4.0, MYNN-EDMF provides tendencies for the following "moist" variables: q_c, q_i, and q_v. Other "moist" variables, such as graupel q_g, snow q_s, hail q_h, and rain q_r are not mixed. The other group of "scalar" variables, i.e., q_{nc}, q_{ni}, q_{ng}, q_{ns}, q_{nh}, etc, can be mixed (locally only) in the subroutine *mix4d* located in the PBL driver, which makes use of the eddy diffusivity from the MYNN-EDMF. These scalars are only mixed when the namelist parameter *scalar_pblmix* is = 1. Note that in WRF–ARW, the "moist" arrays have their own separate tendency arrays, but the tendencies for the "scalar" arrays are packaged into the *SCALAR_TEND* array. Current experimental versions of the MYNN-EDMF can also mix the "scalar" arrays, bypassing the need to lean on the exterior subroutine *mix4d,* and allowing use of the mass-flux scheme for consistent nonlocal mixing. This requires setting the namelist parameter *bl_mynn_mixscalars* to 1, which automatically set *scalar_pblmix* to 0. This experimental code has recently been integrated into NCAR's WRF-ARW version 4.1 repository.

For the Thompson aerosol-aware microphysics scheme, there are two extra scalar variables, *qnwfa* and *qnifa*, which are mixed in *mix4d* subroutine along with the other number concentrations when *scalar_pblmix* is = 1. These aerosols can alternatively be mixing within the MYNN-EDMF when *bl_mynn_mixscalars* is set to 1. Currently there is no consideration of the aerosol effects on the SGS clouds in the MYNN-EDMF.

6.4 Fog Settling

The original MYNN included the gravitational settling of cloud droplets as described in Nakanishi (2000), which used the formulation of the cloud droplet deposition velocity proposed by Duynkerke (1991). In older versions of WRF–ARW (pre-v3.7), this physical process was only represented in the MYNN PBL scheme. The namelist parameter, *grav_settling* (inactive by default), activates this physical process. In more recent versions of WRF–ARW, this process was removed from the MYNN and placed in a new module (phys/module_bl_fogdes.F) called within the PBL driver, so that it can be used in combination with any PBL scheme. As part of the new fog deposition module, a new vegetation-dependent deposition velocity based on Katata et al. (2008) was added to impact the deposition velocity in the lowest model level in advective situations. Note that *grav_settling* should be set to zero (kept inactive) when using the Thompson microphysics scheme, since this process is already included. Consult with your local microphysicist to see if this process is already included in other microphysics schemes.

When *grav_settling = 1* (activated), the tendency for q_c, calculated in phys/module_bl_fogdes.F, is added to the PBL tendency array *RQCBLTEN*. Thus, an analysis of moisture tendencies from the MYNN-EDMF (or any other scheme) should only be undertaken with *grav_settling* = 0, so as to isolate the contribution from the MYNN-EDMF.

6.5 Orographic Drag

The MYNN-EDMF is not dependent upon any fields from the orographic drag scheme in WRF–ARW; however, the drag scheme needs KPBL and PBLH, which are both calculated in the MYNN-EDMF (or other PBL schemes). The tendencies from the orographic drag scheme are added to PBL-tendency arrays *RUBLTEN* and *RVBLTEN*, which are then added to the other momentum tendencies in the subroutine phys/module_physics_addtendc.F. Thus, to analyze the momentum tendencies from the MYNN-EDMF (or any other PBL scheme) in isolation, do not activate an orographic drag scheme (set *gwd_opt* = 0, in dynamics section of namelist).

7. Description of Output Fields

7.1 Hybrid Diagnostic Boundary-Layer Height (PBLH)

The modifications presented above require the MYNN to use z_i as an internal variable, so we must give extra care for an accurate diagnostic for z_i. Results from Lemone et al. (2013, 2014) show that a potential temperature-based definition of z_i is generally accurate for convective boundary layers, while TKE-based definitions perform well for stable boundary layers; therefore, we implemented a hybrid definition.

We took a virtual liquid water and ice potential temperature-based version of the boundary layer height definition, $z_{i\theta}$, of Nielsen-Gammon et al. (2008). This algorithm first searches the lowest 200 m of the atmosphere to find the height of the minimum virtual liquid and ice potential temperature (θ_{vli_min}). This helps to reduce the impact of surface-based superadiabatic layers on the diagnosis of $z_{i\theta}$. Then $z_{i\theta}$ is determined to be the height at which $\theta_{vli} = \theta_{vli\_min} + \Delta\theta_{vli}$, where $\Delta\theta_{vli}$ is set to 0.75 K over water and 1.25 K over land. We took the TKE-based definition of boundary-layer height (z_{iTKE}) to be the height at which the TKE at the surface, TKE_{sfc}, decreases to below a

threshold value, TKE_{min}. We chose the quantity TKE_{min} to be 5% of the TKE_{sfc} —a criterion chosen independently by Kosović and Curry (2000) as well as used in Cuxart et al. (2006). TKE_{min} is also bound to be greater than 0.02 $m^2 s^{-2}$ in the case of stagnant cold pools, where the lack of a lower limit can result in an excessively large estimate of z_{iTKE}.

We blended the two definitions such that $z_{i\theta}$ will dominate for neutral and unstable conditions (when $z_{i\theta} > 200$ m), while z_{iTKE} will dominate for stable conditions ($z_{i\theta} < 200$ m), where $z_{i\theta}$ is used as an indicator of stability. We used a hyperbolic tangent for blending the two definitions, similar to equations 12a and b, but in (12b), we replaced z_i with $z_{i\theta}$, set Δz to 200 m, and set the blending height determined by the denominator in the hyperbolic tangent argument to 400 m. This hybrid algorithm has been shown to accurately diagnose the boundary-layer height throughout a diurnal cycle (Fitch et al. 2013).

7.2 10-m Wind (*U10*, *V10*)

The 10-m zonal and meridional wind components, *U10* and *V10*, respectively, are two-dimensional fields computed by using a neutral-log in the MYNN surface-layer scheme (not described here):

$$U10 = U_1 \log(10/z_0)/\log(z_1/z_0)$$
$$V10 = V_1 \log(10/z_0)/\log(z_1/z_0)$$

Where U_1 and V_1 are the wind components valid at the middle of the lowest atmospheric model layer, z_1 is equal to half the depth of the first model layer, and z_0 is the aerodynamic roughness length. Note that prior to WRF–ARWv4.0, we set *U10* and *V10* equal to the wind components at the lowest model level if the height of the first model level z_1 was $7 < z_1 < 13$ m. We removed this and now use the neutral-log form.

7.3 Maximum Mass Flux (*MAXMF*)

MAXMF is a two-dimensional diagnostic output from the mass-flux scheme. We calculated this field by searching for the maximum mass flux at levels for all plumes active in a particular model grid column. There is no level information kept to describe the height at which the maximum mass flux occurred. However, to provide information on whether any of the plumes in a grid column had condensed or not, we kept the maximum mass flux positive if any plume reached the lifting condensation level and produced a shallow-cumulus cloud. We multiplied the maximum mass flux by -1 if no plumes condensed, since it is only a diagnostic output and does not impact the functionality of the scheme.

7.4 Number of Plumes/Updrafts Active (*NUPDRAFTS*)

NUPDRAFTS is a two-dimensional integer field which shows how many updrafts (or plumes) are active at the particular time step written out. Since the plume numbers (1, 2, …, 10) correspond to plume widths (100, 200, …, 1000 m), the number n at a particular location means all plume sizes less than or equal to n*100 are active.

7.5 *k* Index of Highest-Rising Plume (*KTOP_SHALLOW*)

KTOP_SHALLOW is a two-dimensional integer field which shows the *k*-index of the highest-reaching plume at each horizontal location. This always corresponds to the largest plume active within a grid column, since the entrainment rate is inversely proportional to the plume diameter. Note that this field is shared with the Grell-Freitas shallow-cumulus scheme, which should be shut off by setting namelist parameter *ishallow* to 0 if using the Grell-Freitas convection scheme with the MYNN-EDMF.

8. Code Description

Dr. Mikio Nakanishi freely offered the original code. Mariusz Pagowski then transformed this code into Fortran 90 with WRF-specific code compliance. Joseph Olson, Jaymes Kenyon, Wayne Angevine, and Kay Sušelj then introduced many subsequent modifications and additional features.

For WRF–ARW-related context, the boundary-layer schemes are called after the radiation, surface- layer, and land-surface models. These three schemes collectively calculate the necessary input for the boundary-layer schemes beyond the basic state variables: u_*, *HFX*, *QFX*, *z/L*, and *RTHRATEN* (radiation temperature tendency). After the boundary-layer scheme is called, the gravity wave drag and urban schemes are called, then the convection scheme and finally, the microphysics scheme. After making all the calls to all of the physics schemes, the horizontal diffusion, advection, and filters are applied at the end of the time step.

Within the MYNN-EDMF, there is a dependency check for the first time step. If true, a three-dimensional initialization loop is entered. Within this loop, several arrays are initialized and *k*-

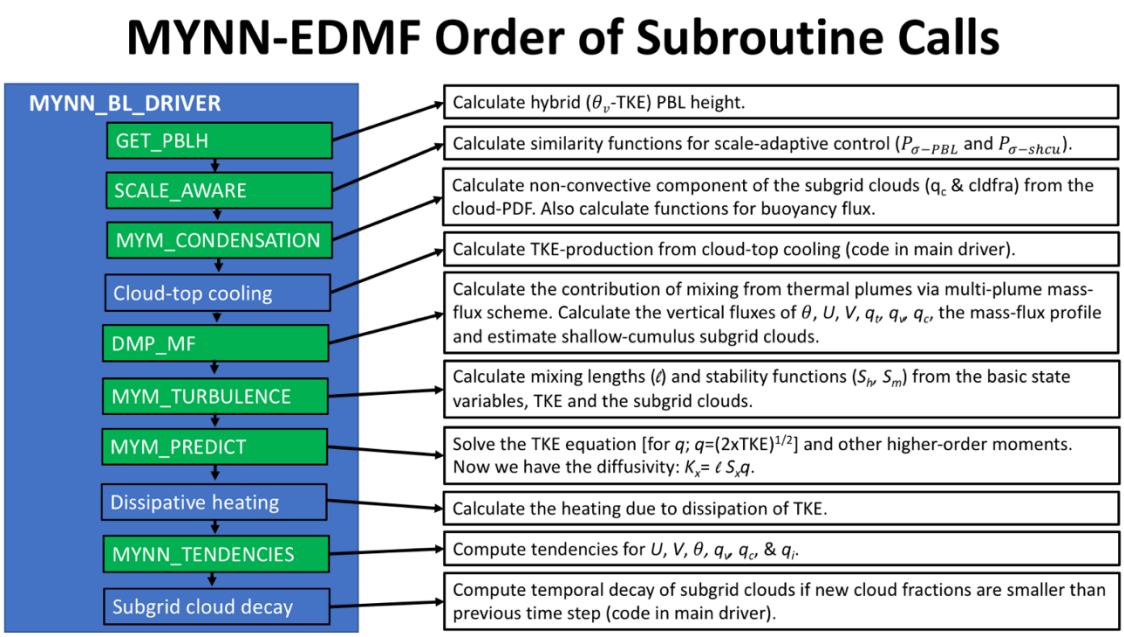

Figure 7. The order of subroutines within the MYNN-EDMF. The green rectangles within the main subroutine (MYNN_BL_DRIVER) represent subroutine calls. The blue rectangles represent tasks coded within the main driver. A brief description is shown on the right.

oriented (vertical) subroutines are called at every *i* and *j* point, corresponding to the x- and y-directions, respectively. We describe the function of these three subroutines below:

- **GET_PBLH**: Calculates the hybrid θ_{vli}-*TKE* PBL height.
- **SCALE_AWARE**: Calculates the similarity functions, $P_{\sigma\text{-}PBL}$ and $P_{\sigma\text{-}shcu}$, to control the scale-adaptive behavior for the local and nonlocal components, respectively.
- **MYM_INITIALIZE**: initializes the mixing length, TKE, θ'^2, q'^2, and $\theta' q'$. These variables are calculated after obtaining prerequisite variables by calling the following subroutines from within **MYM_INITIALIZE**:
    - **MYM_LEVEL2**: Calculates the level 2, non-dimensional wind shear G_M and vertical temperature gradient G_H as well as the level 2 stability functions S_h and S_m.
    - **MYM_LENGTH**: calculates the mixing lengths.

After initializing all required variables, the regular procedures performed at every time step are were ready for execution. The main subroutine **MYNN_BL_DRIVER** encompasses the majority of the subroutines that comprise the procedures that ultimately solve for tendencies of U, V, θ, q_v, q_c, and q_i. We show the full order of procedure/subroutines called within **MYNN_BL_DRIVER** in figure 7.

We outline the set of procedures below:

- **GET_PBLH**: Calculates the hybrid θ_{vli}-*TKE* PBL height diagnostic.
- **SCALE_AWARE**: Calculates the similarity functions, $P_{\sigma\text{-}PBL}$ and $P_{\sigma\text{-}shcu}$, to control the scale-adaptive behavior for the local and nonlocal components, respectively.
- **MYM_CONDENSATION**: Calculates the nonconvective component of the subgrid cloud fraction and mixing ratio as well as the functions used to calculate the buoyancy flux. Different cloud PDFs can be selected by use of the namelist parameter *bl_mynn_cloudpdf*, as described in section 4.
- After the subgrid clouds are calculated, the buoyancy production of TKE from cloud-top cooling is calculated from a section of code within the main driver subroutine. This is only activated when the hard-coded parameter *bl_mynn_topdown* (located near the beginning of module_bl_mynn.F) is set to 1. This is set to 0 by default.
- **DMP_MF**: (Formerly STEM_MF) Calculates the nonlocal turbulent transport from the dynamic multiplume mass-flux scheme as well as the shallow-cumulus component of the subgrid clouds. Note that this mass-flux scheme is called when the namelist parameter *bl_mynn_edmf* is set to 1 (recommended). If *bl_mynn_edmf* is set to 2, an alternative (and unfinished) mass-flux scheme, adapted from the TEMF PBL scheme (Angevine et al. 2010) is used. This alternative mass-flux scheme resides in the subroutine **TEMF_MF**, but may be removed from the code in the future.
- **MYM_TURBULENCE**: First, two subroutines are called within this subroutine to collect the necessary variable to carry out successive calculations:
    - **MYM_LEVEL2**: Calculates the level 2 nondimensional wind shear G_M and vertical temperature gradient G_H as well as the level 2 stability functions S_h and S_m.
    - **MYM_LENGTH**: calculates the mixing lengths.
    - Then stability criteria from Helfand and Labraga (1989) are applied.
    - The stability functions for level 2.5 or level 3.0 are calculated.
    - If level 3.0 is used, counter-gradient terms are calculated.

    - Production terms of TKE, θ'^2, q'^2, and $\theta' q'$ are calculated.
    - Eddy diffusivity K_h and eddy viscosity K_m are calculated.
    - TKE budget terms are calculated (if the namelist parameter *bl_mynn_tkebudget* is set to True).
- **MYM_PREDICT**: solves for TKE and, if running level 3.0, also solves for θ'^2, q'^2, and $\theta' q'$ for the following time step.
- After the TKE is updated, the heating due to dissipation of TKE is calculated if the hard-coded parameter *dheat_opt* (located near the beginning of module_bl_mynn.F) is set to 1. This is set to 1 by default.
- **MYNN_TENDENCIES**: solve for tendencies of U, V, θ, q_v, q_c, and q_i.
- Lastly, there is a section of code within the main driver subroutine that computes the temporal decay of diagnostic subgrid cloud. This allows the diagnostic subgrid clouds to persist for an eddy turnover timescale.

9. Summary, Other Notes, and Future Work

Mariusz Pagowski (NOAA/GSD) originally integrated the MYNN PBL scheme into WRF–ARWv3.1 in 2009. The MYNN was selected for a variety of reasons: (1) improved mixing-length formulation, (2) closure constants diagnosed from LES, (3) use of a cloud PDF for the representation of moist turbulent processes, (4) the option to use the level-3 closure, and (5) at the beginning of this integration effort, there were only two PBL schemes in WRF–ARW. After considerable testing, we determined the MYNN to be a candidate for use within the operational RAP and HRRR. In subsequent versions (e.g., v3.4.1), we deemed the performance of the MYNN within the RAP/HRRR physics suite sufficient to be chosen as the successor to the Mellor-Yamada-Janjić (MYJ; Janjić 2002) PBL scheme, which was used in first version of the operational Rapid Refresh (RAPv1). Despite the improvements inherited by switching to the MYNN, it has undergone further developments over the years in an attempt to improve bias characteristics in the RAP/HRRR, as revealed by extensive model validation for a wide variety of forecast metrics, including near-surface variables, vertical profiles of temperature, winds, and humidity from radiosondes and aircraft data, precipitation, radar reflectivity, cloud ceilings, and downward shortwave radiation. We have documented all significant modifications within this manuscript with the exception of the surface-layer physics, which we will document elsewhere.

PBL scheme development within the context of the RAP/HRRR forecast system (or any defined physics suite) brings the challenge of error attribution uncertainty. Interactions between the parameterized turbulent mixing and other model components, such as radiation, land-surface model, convection, and microphysics can cause feedbacks that lead to ambiguity in assessing the true source of errors. Model validation-driven changes made to any of these other components may lead to behavioral changes in the MYNN-EDMF, which will then need to be requantified. Prescribed quantities in the surface data, such as land-use, topography, albedo, surface roughness lengths, etc. can also impact the mean bias characteristics, further complicating the attribution of model errors. Finally, in hourly-cycled forecast systems like the RAP and HRRR, the behavior of the model spin-up during the first forecast hour, the data assimilation system itself, and the rebalancing of the post-assimilation, three-dimensional atmospheric state can all impact the forecast skill, making error attribution even more difficult. Model validation at very short range

(0–3 h), versus longer ranges can sometimes help to differentiate errors from the model physics and data assimilation, but only long-term testing with different surface data sources can help elucidate the errors caused by the various prescribed surface datasets. To distinguish the true sources of the errors from the boundary-layer scheme from the rest of the forecast system, we complement our 3-D testing with isolated process-oriented studies in simpler frameworks, like single-column modeling (SCM), with varying degrees of interacting physics and/or specified states/fluxes. Some results from SCM testing of the MYNN-EDMF are reported by Angevine et al. (2018). Further testing in simplified frameworks or the fully-cycled RAP and HRRR will undoubtedly drive more changes to future versions of the MYNN-EDMF. We've included some notes on ongoing and future work below:

i. *Further work on turbulence linked to cloud-top cooling*

It remains unclear whether or not a nonlocal production of TKE (section 2.1) is sufficient to represent the turbulent mixing associated with cloud-top cooling. This mechanism keeps the eddy-diffusivity coefficient nonzero in stable inversions, but still relies on the traditional tridiagonal solver (local diffusion calculation) to represent this mixing. Other approaches, such as explicit entrainment or the use of the mass-flux method applied to downdrafts may better parameterize the impacts of destabilized parcels in stratocumulus environments.

ii. *Adding precipitation processes to the mass-flux scheme*

The widest plumes currently parameterized in the mass-flux scheme used in the MYNN-EDMF are meant to represent 1000-m plumes. Plumes this size are on the large end of the shallow-cumulus spectrum and may arguably be considered midlevel convection, which can be associated with precipitation, especially in the marine boundary layer. Without a proper representation of parameterized precipitation, large fluxes of liquid water may produce high relative humidity biases between 850–700 hPa with consequential cloud-cover biases. To reduce the chances of these biases appearing, the inclusion of shallow-cumulus precipitation processes may be a necessary next step.

iii. *Further work on SGS clouds*

The diagnostic statistical schemes currently in the MYNN-EDMF assume that the PDF variance responds to changes in mixing length and/or vertical gradients of prognostic variables. However, in reality, the sources of the PDF variance can be due to other subgrid-scale processes, such as advective or convective transport. Moreover, a diagnostic approach results in an instantaneous adjustment of the SGS macrophysical properties, which may lead to unrealistic fluctuations and can spread noise into other components of the model through physical interactions. A more physically suitable method may be to replace the diagnostic relationship with a prognostic approach. Examples of PDF-based prognostic schemes include Tompkins (2002) or the PC2 scheme (Wilson et al. 2008). More expensive prognostic schemes that incorporate subgrid-scale vertical motion have been developed (Lappen and Randall 2001; Larson and Golaz 2005). With some prognostic higher-order moments already available in the MYNN when run at level-3, an extension to a prognostic SGS cloud approach may be a computationally feasible next step.

Acknowledgments. The authors would like to thank Dr. Mikio Nakanishi for sharing the original version of the MYNN PBL scheme and offering helpful insight and advice as the scheme was developed in WRF-ARW. Funding for this work was provided by many sources, each helping to develop different components of the MYNN-EDMF scheme. These agencies/programs include NOAA's Atmospheric Science for Renewable Energy (ASRE) program, the Federal Aviation Administration (FAA), NOAA's Next Generation Global Prediction System (NGGPS), and the U.S. DOE Office of Energy Efficiency and Renewable Energy Wind Energy Technologies Office. The views expressed are those of the authors and do not necessarily represent the official policy or position of any funding agency. We are grateful to the National Center for Atmospheric Research Mesoscale and Microscale Meteorology Laboratory (http://www.mmm.ucar.edu/wrf/users), which is responsible for the Weather Research and Forecasting Model, and specifically grateful for help from Jimy Dudhia, Wei Wang, and Dave Gill.

Appendix: Summary of MYNN-EDMF Namelist Options

Namelist Option (&physics)	Value	Description and Default Configuration (as of WRF–ARWv4.0)
bl_mynn_mixlength	0	Original form from NN2009
	1	HRRR operational form 201609–201807. Designed to work without the mass-flux scheme.
	2	HRRR operational form 201807–present. Designed to be compatible with mass-flux scheme activated. (default)
bl_mynn_cloudpdf	0	Use Sommeria-Deardorff subgrid cloud PDF
	1	Use Kuwano-Yoshida subgrid cloud PDF
	2	Use modified Chaboureau-Bechtold subgrid cloud PDF (default)
bl_mynn_edmf	0	Deactivate mass-flux scheme
	1	Activate dynamic multiplume mass-flux scheme (default)
bl_mynn_edmf_mom	0	Deactivate momentum transport in mass-flux scheme (default)
	1	Activate momentum transport in dynamic multiplume mass-flux scheme. bl_mynn_edmf must be set to 1.
bl_mynn_edmf_tke	0	Deactivate TKE transport in mass-flux scheme (default)
	1	Activate TKE transport in dynamic multiplume mass-flux scheme. bl_mynn_edmf must be set to 1.
bl_mynn_cloudmix	0	Deactivate the mixing of any water species mixing ratios
	1	Activate the mixing of all water species mixing ratios (default)
bl_mynn_mixqt	0	Mix individual water species separately (default)
	1	DO NOT USE
bl_mynn_tkeadvect	False	Deactivate TKE advection (default)
	True	Activate TKE advection
grav_settling	0	Deactivate gravitational settling of fog (default)
	1	Activate gravitational settling of fog. Do not use this option if cloud-droplet settling is handled within the microphysics scheme.
icloud_bl	0	Deactivate coupling of subgrid clouds to radiation
	1	Activate subgrid cloud coupling to radiation (highly suggested)

Table 1. Description of the WRF–ARW namelist options pertaining to the MYNN-EDMF.

References

Abdella, K. and N. McFarlane, 1997: A new second-order turbulence closure scheme for the planetary boundary layer. *J. Atmos. Sci.,* **54,** 1850–1867.

Angevine, W.M., H. Jiang, and T. Mauritsen, 2010: Performance of an eddy diffusivity–mass flux scheme for shallow cumulus boundary layers. *Mon. Wea. Rev.,* **138**, 2895–2912, doi:10.1175/2010MWR3142.1

Angevine, W. M., J. B. Olson, J. S. Kenyon, W. Gustafson, S. Endo, K. Sušelj, 2018: Shallow cumulus in a mesoscale model evaluated with the LASSO framework. *Mon. Wea. Rev.*, re-submitted.

Benjamin, S. G., S. S. Weygandt, J. M. Brown, M. Hu, C. R. Alexander, T. G. Smirnova, J. B. Olson, E. P. James, D. C. Dowell, G. A. Grell, H. Lin, S. E. Peckham, T. L. Smith, W. R. Moninger, J. S. Kenyon, and G. S. Manikin, 2016: A North American hourly assimilation and model forecast cycle: the Rapid Refresh. *Mon. Wea. Rev.,* **144**, 1669–1694, doi:10.1175/MWR-D-15-0242.1

Benner, T. C., and J. A. Curry, 1998: Characteristics of small tropical cumulus clouds and their impact on the environment. *J. Geophys. Res.*, **103**, 28,753–28,767.

Blackadar, A. K., 1962: The vertical distribution of wind and turbulent exchange in a neutral atmosphere. *J. Geophys. Res.*, **67**, 3095-3102.

Bougeault, P. and P. Lacarrere, 1989: Parameterization of orography-induced turbulence in a mesobeta-scale model. *Mon. Wea. Rev*., **117**, 1872–1890, doi:10.1175/ 1520-0493(1989)117,1872:POOITI.2.0.CO;2.

Brast, M., R. A. J. Neggers, and T. Heus, 2016: What determines the fate of rising parcels in a heterogeneous environment? *J. Adv. Model. Earth Syst.*, **8**, 1674–1690, doi:10.1002/2016MS000750.

Bretherton, C. S., J. R. McCaa, and H. Grenier, 2004: A new parameterization for shallow cumulus convection and its application to marine subtropical cloud-topped boundary layers. Part I: Description and 1D results. *Mon. Wea. Rev.,* **132**, 864–882, doi:10.1175/1520-0493(2004)132<0864:ANPFSC>2.0.CO;2

Canuto, V. M., Y. Cheng, A. M. Howard, and I. N. Easu, 2008: Stably stratified flows: A model with no Ri(cr). *J. Atmos. Sci.*, **65**, 2437–2447, doi:10.1175/2007JAS2470.1.

Chaboureau, J.-P., and P. Bechtold, 2002: A simple cloud parameterization derived from cloud resolving model data: Diagnostic and prognostic applications. *J. Atmos. Sci.*, **59**, 2362–2372.

Chaboureau, J.-P., and P. Bechtold, 2005: Statistical representation of clouds in a regional model and the impact on the diurnal cycle of convection during Tropical Convection, Cirrus and Nitrogen Oxides (TROCCINOX). *J. Geophys. Res.*, **110**, D17103, doi:10.1029/2004JD005645.

Cheinet, S., 2003: A multiple mass-flux parameterization for the surface-generated convection. Part I: Dry plumes. *J. Atmos. Sci.,* **60**, 2313–2327, doi:10.1175/1520-0469(2003)060<2313:AMMPFT>2.0.CO;2

Cuxart, J., P. Bougeault, and J.-L. Redelsperger, 2000: A turbulence scheme allowing for mesoscale and large-eddy simulations. *Q. J.R. Meteorol. Soc*., **126**: 1-30.

Cuxart, J., A. A. M. Holtslag, R. J. Beare, E. Bazile, A. Beljaars, A. Cheng, L. Conangla, M. B. Ek, F. Freedman, R. Hamdi, A. Kerstein, H. Kitagawa, G. Lenderink, D. Lewellen, J. Mailhot, T. Mauritsen, V. Perov, G. Schayes, G. J. Steeneveld, G. Svensson, P. Taylor, W. Weng, S. Wunsch, K. M. Xu, 2006: Single-column model intercomparison for a stably stratified atmospheric boundary layer. *Boundary-Layer Meteorol.*, **118**, 273–303.

de Roode, S. R., A. P. Siebesma, H. J. Jonker, and Y. de Voogd, 2012: Parameterization of the vertical velocity equation for shallow cumulus clouds. *Mon. Wea. Rev.,* **140**,2424–2436, doi:10.1175/MWR-D-11-00277.1

Deardorff, J. W., 1970: Convective velocity and temperature scales for the unstable planetary boundary layer and for Rayleigh convection. *J. Atmos. Sci.,* **27**, 1211–1213.

Deardorff, J. W., 1980: Cloud-top entrainment instability. *J. Atmos. Sci.*, **37**, 131–147.

Duynkerke, P. G. and Driedonks, A. G. M., 1987: A model for the turbulent structure of the stratocumulus-topped atmospheric boundary layer. *J. Atmos. Sci.* **44**, 43–64.

Duynkerke, P. G., 1991: Radiation fog: a comparison of model simulation with detailed observations, *Mon. Wea. Rev.* **119**, 324–342.

Esau, I. N. and Ø. Byrkjedal, (2007). Application of a large-eddy simulation database to optimisation of first-order closures for neutral and stably stratified boundary layers. *Boundary Layer Meteorology,* **125**(2), 207-225. doi:10.1007/s10546-007-9213-6

Fitch, A. C., J. K. Lundquist, and J. B. Olson, 2013: Mesoscale influences of wind farms throughout a diurnal cycle. *Mon. Wea. Rev.*, **141**, 2173–2198, doi:10.1175/MWR-D-12-00185.1.

Furuichi, N., T. Hibiya, and Y. Niwa, 2012: Assessment if turbulence closure models for resonant inertial response in the oceanic mixed layer using a large eddy simulation model. *J. Oceanography.*, **68**, 285-194.

Galperin, B., S. Sukoriansky, and P. S. Anderson, 2007: On the critical Richardson number in stably stratified turbulence. *Atmos. Sci. Lett.*, **8**, 65–69, doi:10.1002/asl.153.

Gambo, K., 1978: Notes on the turbulence closure model for atmospheric boundary layers. *J. Meteor. Soc. Japan*, **56**, 466–480.

Garratt, J. R., 1992: The Atmospheric Boundary Layer. Cambridge University Press, 316 pp.

Golaz, J., V. E. Larson, and W. R. Cotton, 2002: A PDF-based model for boundary layer clouds. Part I: method and model description. *J. Atmos. Sci.,* **59**, 3540–3551, doi:10.1175/1520-0469(2002)059<3540:APBMFB>2.0.CO;2

Grenier, H., and C. S. Bretherton, 2001: A moist PBL parameterization for large-scale models and its application to subtropical cloud-topped marine boundary layers. *Mon. Wea. Rev*, **129,** 357–377.

Ha, K.-J. and L. Mahrt, 2001: Simple inclusion of z-less turbulence within and above the modeled nocturnal boundary layer. *Mon. Wea. Rev., **129***(8), 2136-2143.

Han, Jongil and Christopher S. Bretherton, 2019: Scale-aware TKE-based moist eddy-diffusivity mass-flux (EDMF) parameterization for vertical turbulent mixing interacting with cumulus convection. *Weather and Forecasting*, submitted.

Helfand, H.M. and J.C. Labraga, 1988: Design of a nonsingular level 2.5 Second-order closure model for the prediction of atmospheric turbulence. *J. Atmos. Sci.,* **45**,113–132, doi:10.1175/1520-0469(1988)045<0113:DOANLS>2.0.CO;2

Hobbs, P. V., 1974: High concentrations of ice particles in a layer cloud. *Nature*, **251,** 694–696, doi:10.1038/251694b0

Honnert R., V. Masson, and F. Couvreux, 2011: A diagnostic for evaluating the representation of turbulence in atmospheric models at the kilometric scale. *J. Atmos. Sci*., **68**, 3112–3131.

Ito, J., H. Niino, M. Nakanishi, and C.-H. Moeng, 2015: An extension of the Mellor–Yamada model to the terra incognita zone for dry convective mixed layers in the free convection regime. *Boundary-Layer Meteorol*, **157**, 23-43. doi:10.1007/s10546-015-0045-5

Janjić, Z., 2002: Nonsingular implementation of the Mellor–Yamada level 2.5 scheme in the NCEP meso model. NCEP Office Note No. 437, pp. 60

Katata, G., H. Nagai, T. Wrzesinsky, O. Klemm, W. Eugster, and R. Burkard, 2008: Development of a land surface model including cloud water deposition on vegetation. *J. Appl. Meteor. Climatol.,* **47**, 2129–2146, doi:10.1175/2008JAMC1758.1

Kim. J. and L. Mahrt, 1992: Simple formulation of turbulent mixing in the stable free atmosphere and nocturnal boundary layer. *Tellus*, **44A**, 381-394.

Kitamura, Y., 2010: Modifications to the Mellor-Yamada-Nakanishi-Niino (MYNN) model for the stable stratification case. *J. Meteor. Soc. Japan*, **88**, 857–864, doi:10.2151/ jmsj.2010-506.

Köhler, M., M. Ahlgrimm, and A. Beljaars, 2011: Unified treatment of dry convective and stratocumulus-topped boundary layers in the ECMWF model. *Q. J. R. Meteorol. Soc.*, **137**, 43-57.

Kosović, B. and J. A. Curry, 2000: A large eddy simulation study of a quasi-steady, stably stratified atmospheric boundary layer. *J. Atmos. Sci.*, **57**, 1052–1068, doi:10.1175/ 1520-0469(2000)057,1052:ALESSO.2.0.CO;2.

Kurowski, M.J. and J. Teixeira, 2018: A scale-adaptive turbulent kinetic energy closure for the dry convective boundary layer. *J. Atmos. Sci.,* **75**, 675–690, doi:10.1175/JAS-D-16-0296.1

Kuwano-Yoshida, A., Enomoto, T. and Ohfuchi, W., 2010: An improved PDF cloud scheme for climate simulations. *Q.J.R. Meteorol. Soc*., **136**: 1583-1597. doi:10.1002/qj.660

Lemone, M. A. and W. T. Pennell, 1976: The relationship of trade wind cumulus distribution to subcloud layer fluxes and structure. *Mon. Wea. Rev.,* **104**, 524–539, doi:10.1175/1520-0493(1976)104<0524:TROTWC>2.0.CO;2

Lemone, M. A., M. Tewari, F. Chen, and J. Dudhia, 2013: Objectively determined fair-weather CBL depths in the ARW-WRF model and their comparison to CASES-97 observations. *Mon. Wea. Rev.*, **141**, 30–54, doi:10.1175/MWR-D-12-00106.1.

Lemone, M. A., M. Tewari, F. Chen, and J. Dudhia, 2014: Objectively determined fairweather NBL features in ARW-WRF and their comparison to CASES-97 observations. *Mon. Wea. Rev*., **142**, 2709–2732, doi:10.1175/MWR-D-13-00358.1.

Lenderink, G. and A. A. M. Holtslag, 2004: An updated length-scale formulation for turbulent mixing in clear and cloudy boundary layers. *Q. J. R. Meteorol. Soc*., **130**, 3405–3427. doi: 10.1256/qj.03.117

Lenderink G. and A. A. M. Holtslag, 2000: Evaluation of the kinetic energy approach for modeling turbulent fluxes in stratocumulus. *Mon. Wea. Rev.,* **128**, 244–258.

Lock, A. and J. Mailhot, 2006: Combining non-local scalings with a TKE closure for mixing in boundary layer clouds. *Boundary-Layer Meteorol*. **121**, 313–338.

Mahrt, L. and D. Vickers, 2003: Formulation of turbulent fluxes in the stable boundary layer. *J. Atmos. Sci.,* **60**, 2538–2548, doi:10.1175/1520-0469(2003)060<2538:FOTFIT>2.0.CO;2

Mauritsen, T., G. Svensson, S. S. Zilitinkevich, I. Esau, L. Enger, and B. Grisogono, 2007: A total turbulent energy closure model for neutrally and stably stratified atmospheric boundary layers. *J. Atmos. Sci.*, **64,** 4113–4126.

Mellor, G. L., 1977: The Gaussian cloud model relations. *J. Atmos. Sci*, **34**, 356-358.

Mellor, G. L. and T. Yamada, 1974: A hierarchy of turbulence closure models for planetary boundary layers. *J. Atmos. Sci.*, **31**, 1791–1806, doi:10.1175/1520-0469(1974)031,1791: AHOTCM.2.0.CO;2.

Mellor, G. L. and T. Yamada, 1982: Development of a turbulence closure model for geophysical fluid problems. *Rev. Geophys. Space Phys.*, **20**, 851–875, doi:10.1029/RG020i004p00851.

Nakanishi, M., 2000: Large-eddy simulation of radiation fog. *Bound. Layer Meteor.*, **94**, 461-493.

Nakanishi, M., 2001: Improvement of the Mellor–Yamada turbulence closure model based on large-eddy simulation data. *Bound. Layer Meteor.*, **99**, 349–378.

Nakanishi, M. and H. Niino, 2004: An improved Mellor–Yamada level-3 model with condensation physics: Its design and verification. *Bound. Layer Meteor.*, **112**, 1–31.

Nakanishi, M. and H. Niino, 2006: An improved Mellor–Yamada level-3 model: Its numerical stability and application to a regional prediction of advection fog. *Bound. Layer Meteor.*, **119**, 397– 407.

Nakanishi, M. and H. Niino, 2009: Development of an improved turbulence closure model for the atmospheric boundary layer. *J. Meteor. Soc. Japan,* **87,** 895–912, doi:http://dx.doi.org/10.2151/jmsj.87.895.

Neggers, R.A., H.J. Jonker, and A.P. Siebesma, 2003: Size statistics of cumulus cloud populations in large-eddy simulations. *J. Atmos. Sci.,* **60**, 1060–1074, doi:10.1175/1520-0469(2003)60<1060:SSOCCP>2.0.CO;2

Neggers, R. A. J., M. Köhler, and A. Beljaars, 2009: A dual mass flux framework for boundary layer convection. Part I: Transport. *J. Atmos. Sci.*, **66**, 1465–1487.

Neggers, R. A. J., 2015: Exploring bin-macrophysics models for moist convective transport and clouds. *J. Adv. Model. Earth Syst.*, **7**, 2079–2104, doi:10.1002/2015MS000502.

Nichols S. and J. D. Turton, 1986: An observational study of the structure of stratiform cloud sheets: Part II. Entrainment. *Q. J. R. Meteorol. Soc.*, **112** (472), 461-480.

Nielsen-Gammon, J. W. and Coauthors, 2008: Multisensor estimation of mixing heights over a coastal city. *J. Appl. Meteor. Climatol.*, **47**, 27–43, doi:10.1175/2007JAMC1503.1.

Nieuwstadt, F. T. M., 1984: The turbulent structure of the stable, nocturnal boundary layer. *J. Atmos. Sci*., **41**, 2202-2216.

Olson, J. B., and J. M. Brown, 2009: A comparison of two Mellor–Yamada-based PBL schemes in simulating a hybrid barrier jet. Preprints, *23rd Conf. on Weather Analysis and Forecasting/19th Conf. on Numerical Weather Prediction,* Omaha, NE, Amer. Meteor. Soc., JP1.13. [Available online at http://ams.confex.com/ams/pdfpapers/154321.pdf.]

Shin, H. H. and S. Hong, 2013: Analysis of resolved and parameterized vertical transports in convective boundary layers at gray-zone resolutions. *J. Atmos. Sci.,* **70**, 3248–3261, doi:10.1175/JAS-D-12-0290.1

Siebesma, A. P. and J. W. M. Cuijpers, 1995: Evaluation of parametric assumptions for shallow cumulus convection. *J. Atmos. Sci.*, **52**, 650–666.

Siebesma, A. P., C. Bretherton, A. Brown, A. Chlond, J. Cuxart, P. Duynkerke, H. Jiang, M. Khairoutdinov, D. Lewellen, C.-H. Moeng, E. Sanchez, B. Stevens and D. Stevens, 2003: A large-eddy simulation intercomparison study of shallow cumulus convection. *J. Atmos. Sci.*, **60**, 1201–1219.

Siebesma, A. P., P. M. M. Soares, and J. Teixeira, 2007: A combined eddy-diffusivity mass-flux approach for the convective boundary layer, *J. Atmos. Sci.*, **64**, 1230–1248.

Simpson, J. and V. Wiggert, 1969: Models of precipitating cumulus towers, *Mon. Weather Rev.*, **97**, 471–489.

Skamarock, W. C. and Coauthors, 2008: A description of the Advanced Research WRF version 3. NCAR Tech. Note NCAR/TN-4751STR, 125 pp. [Available online at http:// www2.mmm.ucar.edu/wrf/users/docs/arw_v3.pdf.]

Soares, P. M. M., P. M. A. Miranda, A. P. Siebesma, and J. Teixeira, 2004: An eddy-diffusivity/mass-flux parameterization for dry and shallow cumulus convection. *Quart. J. Roy. Meteor. Soc.*, **130**, 3365–3384.

Sommeria, G. and J. W. Deardorff, 1977: Subgrid-scale condensation in models of nonprecipitating clouds. *J. Atmos. Sci.*, **34**, 344–355, doi:10.1175/1520-0469(1977)034,0344:SSCIMO.2.0.CO;2.

Sorbjan, Z., 1991: Evaluation of local similarity functions in the convective boundary layer. *J. Appl. Meteor.*, **30,** 1565–1583.

Stull, R. B., 1988: An Introduction to Boundary Layer Meteorology. Kluwer Academic, 666 pp.

Sun, J., 2011: Vertical variations of mixing lengths under neutral and stable conditions during CASES-99. *J. Appl. Meteor. Climatol.,* **50**, 2030–2041, doi:10.1175/JAMC-D-10-05006.1

Sušelj, K., T. F. Hogan, and J. Teixeira, 2014: Implementation of a stochastic eddy-diffusivity/mass-flux parameterization into the Navy Global Environmental Model. *Weather and Forecasting*, **29**, 1374–1390, doi:10.1175/WAF-D-14-00043.1.

Teixeira, J. and S. Cheinet, 2004: A simple mixing length formulation for the eddy-diffusivity parameterization of dry convection. *Bound. Layer. Meteorology*, **110**: 435–453. doi:10.1023/B:BOUN.0000007230.96303.0d

Teixeira, J. and A. P. Siebesma, 2000: A mass-flux/K-diffusion approach for the parametrization of the convective boundary layer: global model results. Pp. 231– 234 in Proceedings of 14th Symposium on Boundary Layers and Turbulence, (Aspen, Co), American Meteorol. Soc., Boston, USA.

Tian, Y. and Z. Kuang, 2016: Dependence of entrainment in shallow cumulus convection on vertical velocity and distance to cloud edge. *Geophys. Res. Letters*, **43** (8), 4056–4065. doi:10.1002/2016gl069005.

Tompkins, A. M., 2002: A prognostic parameterization for the subgrid-scale variability of water vapor and clouds in large-scale models and its use to diagnose cloud cover. *J. Atmos. Sci.* **59**, 1917–1942.

——, 2008: Cloud Parameterization. In *Proceedings of Workshop on Parametrization of sub-grid physical processes*. ECMWF, Reading, U.K. Available at https://www.ecmwf.int/sites/default/files/elibrary/2009/12778-cloud-parametrization.pdf

Wilson, D. R., A. C. Bushell, A. M. Kerr-Munslow, J. D. Price and C. J. Morcrette, 2008: PC2: A prognostic cloud fraction and condensation scheme. I: Scheme description. *Q. J. R. Meteorol. Soc.*, **134**, 2093–2107. doi:10.1002/qj.333

Wilson, T. H. and R. G. Fovell, 2018: Modeling the evolution and life cycle of radiative cold pools and fog. *Weather and Forecasting*. **33**, 203–220, doi:10.1175/WAF-D-17-0109.1

Witek, M.L., J. Teixeira, and G. Matheou, 2011: An integrated TKE-based eddy diffusivity/mass flux boundary layer closure for the dry convective boundary layer. *J. Atmos. Sci.,* **68**, 1526–1540, doi:10.1175/2011JAS3548.1

Wyngaard, J., O. Coté, and Y. Izumi, 1971: Local free convection, similarity, and the budgets of shear stress and heat flux. *J. Atmos. Sci.*, **28,** 1171–1182.

Xu, K. and D.A. Randall, 1996: A Semiempirical cloudiness parameterization for use in climate models. *J. Atmos. Sci.,* **53**, 3084–3102, doi:10.1175/1520-0469(1996)053<3084:ASCPFU>2.0.CO;2

Yuan, T., 2011: Cloud macroscopic organization: Order emerging from randomness. *Atmos. Chem. Phys.*, **11**(15), 7483–7490, doi:10.5194/acp-11-7483-2011.

Zilitinkevich, S. S., T. Elperin, N. Kleeorin, and I. Rogachevskii, 2007: Energy- and flux-budget (EFB) turbulence closure model for stably stratified flows. Part I: Steady-state, homogeneous regimes. *Bound.-Layer Meteor.*, **125**, 167–191, doi:10.1007/ s10546-007-9189-2.